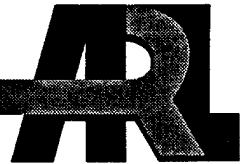


ARMY RESEARCH LABORATORY



Variability of C_N^2 and Wind as Seen by the 50-MHz Radar at WSMR

by Gregory D. Nastrom
St. Cloud State University
St. Cloud, MN

ARL-CR-197

August 1995

19951101 132



DTIC QUALITY INSPECTED 8

Approved for public release; distribution is unlimited.

NOTICES

Disclaimers

The findings in this report are not to be construed as an official Department of the Army position, unless so designated by other authorized documents.

The citation of trade names and names of manufacturers in this report is not to be construed as official Government indorsement or approval of commercial products or services referenced herein.

Destruction Notice

When this document is no longer needed, destroy it by any method that will prevent disclosure of its contents or reconstruction of the document.

REPORT DOCUMENTATION PAGE

Form Approved
OMB No. 0704-0188

Public reporting burden for this collection of information is estimated to average 1 hour per response, including the time for reviewing instructions, searching existing data sources, gathering and maintaining the data needed, and completing and reviewing the collection of information. Send comments regarding this burden estimate or any other aspect of this collection of information, including suggestions for reducing this burden, to Washington Headquarters Services, Directorate for Information Operations and Reports, 1215 Jefferson Davis Highway, Suite 1204, Arlington, VA 22202-4302, and to the Office of Management and Budget, Paperwork Reduction Project (0704-0188), Washington, DC 20503.

1. AGENCY USE ONLY (Leave blank)			2. REPORT DATE	3. REPORT TYPE AND DATES COVERED
			August 1995	Final
4. TITLE AND SUBTITLE			5. FUNDING NUMBERS	
Variability of C_N^2 and Wind as Seen by the 50-MHz Radar at WSMR				
6. AUTHOR(S)				
Gregory D. Nastrom				
7. PERFORMING ORGANIZATION NAME(S) AND ADDRESS(ES)			8. PERFORMING ORGANIZATION REPORT NUMBER	
St. Cloud State University St. Cloud, MN			ARL-CR-197	
9. SPONSORING/MONITORING AGENCY NAME(S) AND ADDRESS(ES)			10. SPONSORING/MONITORING AGENCY REPORT NUMBER	
U.S. Army Research Laboratory Battlefield Environment Directorate Attn: AMSRL-BE White Sands Missile Range, NM 88002-5501			ARL-CR-197	
11. SUPPLEMENTARY NOTES				
Contract Monitor: Frank Eaton				
12a. DISTRIBUTION / AVAILABILITY STATEMENT			12b. DISTRIBUTION CODE	
Approved for public release; distribution is unlimited.			A	
13. ABSTRACT (Maximum 200 words)				
<p>The mean vertical profile of the refractivity turbulence structure constant C_N^2 and its variability with season, time of day, and background weather conditions at White Sands Missile Range (WSMR), NM from approximately 5 to 20 km altitude are described. Observations, taken with a very high frequency 50-MHz profiling radar located at WSMR from January 1991 through April 1994, are used to describe the variability of windspeed, vertical wind shear, spectral width, and volume reflectivity calibrated as C_N^2. C_N^2 is lognormally distributed, shows very small diurnal and interannual variation at all heights, has maximum value in the troposphere during summer, and shows small seasonal variation in the stratosphere. The typical time between statistically independent observations of C_N^2 is approximately 2 h. Daily values of C_N^2 depend strongly on local weather conditions, resulting in a strong correlation of meridional wind direction in the troposphere and indicators of gravity wave activity in the stratosphere. A simple regression model for estimating C_N^2 is presented.</p>				
14. SUBJECT TERMS			15. NUMBER OF PAGES	
radar, wind, turbulence, spectral width, C_N^2			83	
			16. PRICE CODE	
17. SECURITY CLASSIFICATION OF REPORT	18. SECURITY CLASSIFICATION OF THIS PAGE	19. SECURITY CLASSIFICATION OF ABSTRACT	20. LIMITATION OF ABSTRACT	
Unclassified	Unclassified	Unclassified	SAR	

Acknowledgments

Helpful discussions with F. D. Eaton, J. M. Warnock, and T. E. VanZandt are gratefully acknowledged.

Accesion For	
NTIS	CRA&I
DTIC	TAB
Unannounced	<input type="checkbox"/>
Justification	
By	
Distribution /	
Availability Codes	
Dist	Avail and / or Special
A-1	

Contents

Acknowledgments	1
1. Introduction	7
2. Data	9
3. Seasonal and Interannual Variations	13
3.1 <i>Mean Horizontal Winds</i>	13
3.2 <i>Mean Vertical Winds</i>	13
3.3 <i>Spectral Width</i>	19
3.4 C_N^2	19
4. Autocorrelation of Log C_N^2	31
5. Diurnal Variations	37
6. Changes of Log C_N^2 with Background Weather Conditions	47
7. Summary and Conclusions	55
References	57
Appendices	
Appendix A. <i>WSMR Data Inventory</i>	59
Appendix B. <i>Examples of Monthly Charts</i>	61
Distribution	71

Figures

1. Frequency distribution of $\log C_N^2$ at 5.6, 12.1, and 17.0 km, and for the median from 12 to 18 km during 9 winter months. N is the total number of hourly means	11
--	----

2. Frequency distribution of $\log C_N^2$ at 5.6, 12.1, and 17.0 km, and for the median from 12 to 18 km during 11 winter months. The very low values of C_N^2 are spurious	12
3. Seasonal mean profiles of zonal and meridional winds at WSMR	14
4a. Seasonal mean profiles of zonal and meridional winds at WSMR with all seasons plotted together	15
4b. Seasonal means of the vertical shear over 300-m layers of windspeed from individual observations	16
5. Seasonal mean profiles of vertical velocity and its standard deviation over 1-h periods at WSMR. (Note that σ_w is the standard deviation over 1 h.)	17
6. Seasonal mean profiles of vertical velocity and its standard deviation over 1-h periods at WSMR with all seasons plotted together	18
7. Seasonal mean profiles of spectral width at WSMR	20
8. Seasonal mean profiles of spectral width at WSMR with all seasons plotted together	21
9. Seasonal mean profiles of $\log C_N^2$ at WSMR	22
10. Annual mean of $\log C_N^2$ (right side) and seasonal means of $\log C_N^2$ (left side)	23
11. Seasonal mean profiles of standard deviation of hourly means of $\log C_N^2$ (HOURLY) and of standard deviation of $\log C_N^2$ over 1 h (HI FREQ) at WSMR	25
12. Frequency distribution of $\log C_N^2$ at 5.6, 12.1, and 17.0 km, and for the median from 12 to 18 km during 9 spring months.	27
13. Frequency distribution of $\log C_N^2$ at 5.6, 12.1, and 17.0 km, and for the median from 12 to 18 km during 8 summer months	28
14. Frequency distribution of $\log C_N^2$ at 5.6, 12.1, and 17.0 km, and for the median from 12 to 18 km during 9 fall months	29
15. Comparison of individual seasonal means to show interannual variations of $\log C_N^2$	30
16. Autocorrelation function of individual observations of $\log C_N^2$ during January 1993 out to lag 300 min (left side). The right side is out to lag 27 min and in semilogarithmic coordinates	33
17. Autocorrelation function of individual observations of $\log C_N^2$ during February 1993 out to lag 300 min (left side). The right side is out to lag 27 min and in semilogarithmic coordinates	34

18. Autocorrelation function of individual observations of $\log C_N^2$ during July 1993 out to lag 300 min (left side). The right side is out to lag 27 min and in semilogarithmic coordinates	35
19. Diurnal variations of windspeed, spectral width, and $\log C_N^2$ during winter on the beam in the meridional plane	38
20. Diurnal variations of windspeed, spectral width, and $\log C_N^2$ during spring on the beam in the meridional plane	39
21. Diurnal variations of windspeed, spectral width, and $\log C_N^2$ during summer on the beam in the meridional plane	40
22. Diurnal variations of windspeed, spectral width, and $\log C_N^2$ during fall on the beam in the meridional plane	41
23. Diurnal variations of windspeed, spectral width, and σ_w during winter on the beam in the meridional plane	42
24. Diurnal variations of windspeed, spectral width, and σ_w during spring on the beam in the meridional plane	43
25. Diurnal variations of windspeed, spectral width, and σ_w during summer on the beam in the meridional plane	44
26. Diurnal variations of windspeed, spectral width, and σ_w during fall on the beam in the meridional plane	45
27. Vertical profiles of σ_w sorted by hour of the day for each season. Successive 6-h periods have different line types. The mean over 24 h is shown by a bold line	46
28. Correlation and regression relations of $\log C_N^2$ and v at 5.6 km	50
29. Correlation and regression relations of $\log C_N^2$ (the median value from 12 to 18 km) with u at 5.6 km	52
30. Frequency distribution of $\log C_N^2$ at 12 to 18 km for all seasons. Also, the temporal standard deviation (sigma) is included on each panel	53

Appendix Figures

A-1. Monthly inventory of the data available at WSMR during January 1991 through April 1994. (Top) Symbols show the number of hourly means during each month; the solid line shows the average number of observations during each hour, with 20 observations corresponding to full scale. (Bottom) The percent of observations or hourly means (only hours with five or more profiles were analyzed) available as a function of altitude	60
B-1. Horizontal windspeeds plotted as vectors (estimated from the oblique radial velocities assuming the vertical velocity is zero)	63
B-2. Standard deviation of u and v associated with the means in the chart shown in figure B-1, plotted as vectors	64
B-3. Hourly standard deviation of vertical velocity	65
B-4. Vertical profiles of the monthly means of $\log C_N^2$ for the oblique beams. The error bars extend one standard error of the mean from the mean	66
B-5. Deviations of hourly mean $\log C_N^2$ from the monthly means in the chart shown in figure B-4	67
B-6. Vertical profiles of the monthly means for spectral width	68
B-7. Deviations of spectral width from the monthly means in the chart shown in figure B-6	69

Table

1. Regression coefficients for $\log C_N^2$ as a function of u and v at WSMR	51
--	----

1. Introduction

This report describes the mean vertical profile of the refractivity turbulence structure constant C_N^2 and its variability with season, time of day, and background weather conditions at White Sands Missile Range (WSMR), NM. C_N^2 is an important variable for studies of atmospheric turbulence and for the propagation of electromagnetic waves through the atmosphere.

2. Data

Data are from the 50-MHz radar located at WSMR. Details of the radar design and operation, along with examples of the data and a discussion of data quality control procedures, are given by Nastrom and Eaton (1993a, b). The basic period of record available for this study was January 1991 through April 1994. Generally, the radar operated continuously, providing vertical profiles with 150-m resolution from approximately 5 to 20 km every 3 min. The radar has three beams (north, south, and vertical), and each beam is sampled for 1 min in a continuous rotation. The data consisted of complete profiles of the first three moments of each Doppler spectrum (mean Doppler velocity, spectral width, and returned power calibrated as C_N^2). All analyses were made using hourly mean values of the data that survived quality control checks, except the hourly standard deviations of each variable, and the autocorrelation functions of $\log C_N^2$ are based on 3-min observations. Data were collected during 12,251 h with 204,675 profiles recorded. The number of hours of data for each month is given in appendix A, along with the profile of the percent of total data available.

Data continuity was checked by making time-series plots of the hourly mean horizontal and vertical windspeeds and standard deviations, the hourly mean spectral width (used as reported, with no correction for effects such as shear broadening), and the hourly mean C_N^2 . For width and C_N^2 , plots of the monthly means were made and then hourly deviations from the monthly means were plotted to permit easy comparisons among levels in the vertical. Examples of the plots are given in appendix B; a complete file of plots for January 1991 through April 1994 is available for approved requests. These plots show that the radar operated for only 6 h per day (during the night) from October 27, 1991, to June 2, 1992; therefore, these months will not be used in studies of diurnal variations. Some brief periods had anomalously low C_N^2 values; these periods were removed by adding a requirement during data checking that each profile accepted for analyses have at least 25 of the top 50 levels pass all quality control checks.

January 1994 through March 1994 had anomalous C_N^2 values most of the time. For example, figure 1 shows frequency distributions of hourly means of $\log C_N^2$ at 5.6, 12.1, and 17.0 km, and for the median $\log C_N^2$ from 12 to 18 km using data from the 9 winter (December, January, and February) months through December 1993. The distributions appear Gaussian, as expected (past studies such as Hufnagel 1974; Chadwick and Moran 1980; and Nastrom, Gage, and Ecklund 1986 have found that the distribution of C_N^2 appears to be lognormal). Figure 2 shows the frequency distributions for the same data and includes January and February 1994. A bimodal distribution is evident and is due to the spurious values from 1994. Furthermore, a loose electrical connection was found in the radar near this time. Thus, C_N^2 from January to March 1994 will not be used in these climatological studies.

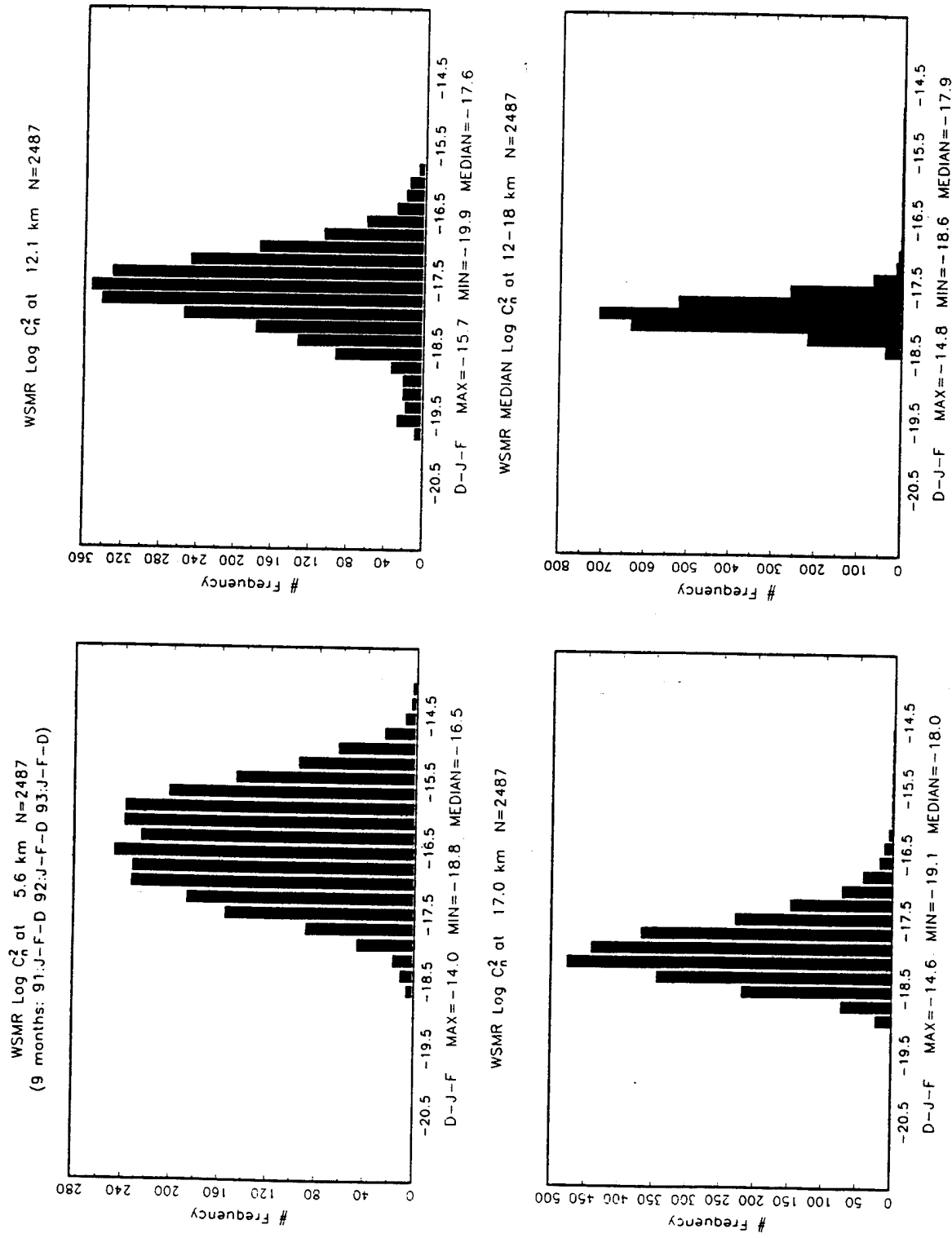
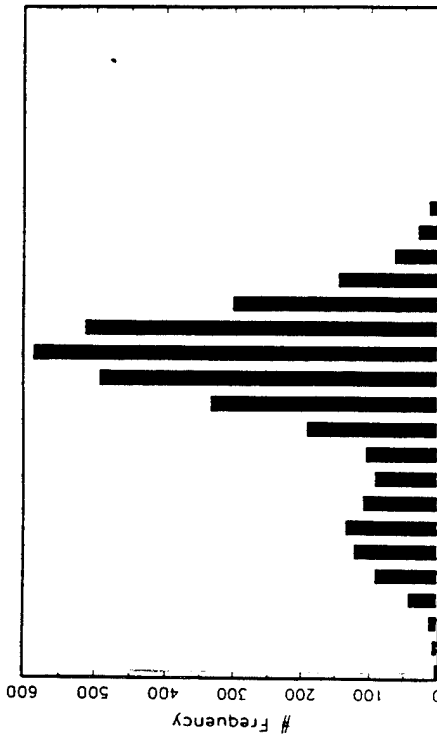
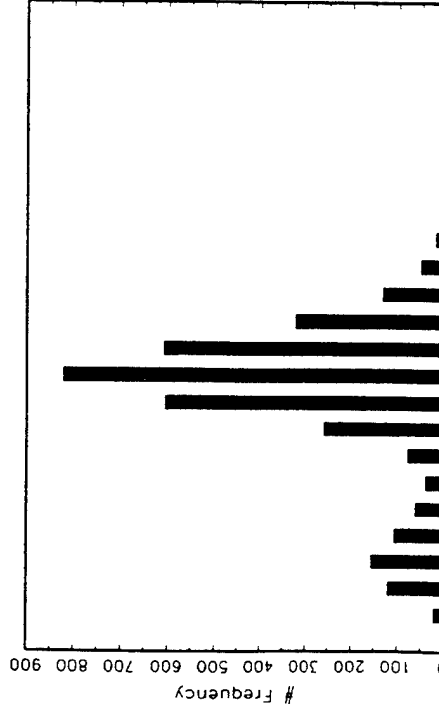


Figure 1. Frequency distribution of $\log C_n^2$ at 5.6, 12.1, and 17.0 km, and for the median from 12 to 18 km during 9 winter months. N is the total number of hourly means.

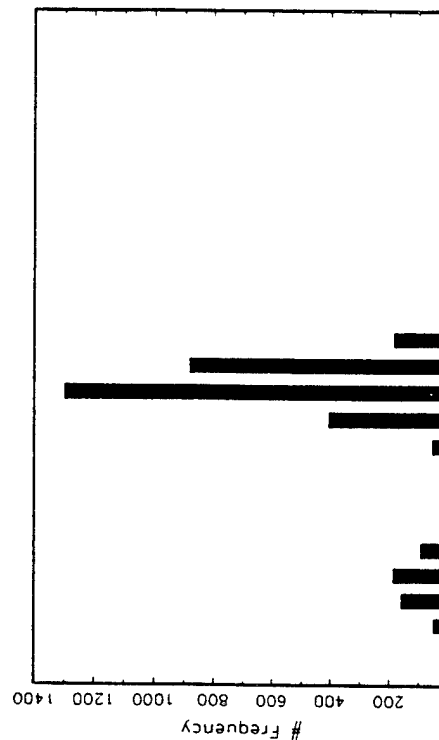
WSMR Log C_n^2 at 5.6 km N=3412
(11 months: 91.J-F-D 92.J-F-D 93.J-F-D 94.J-F)



WSMR Log C_n^2 at 12.1 km N=3412
(11 months: 91.J-F-D 92.J-F-D 93.J-F-D 94.J-F)



WSMR MEDIAN Log C_n^2 at 12-18 km N=3412
(11 months: 91.J-F-D 92.J-F-D 93.J-F-D 94.J-F)



WSMR MEDIAN Log C_n^2 at 12-18 km N=3412
(11 months: 91.J-F-D 92.J-F-D 93.J-F-D 94.J-F)

Figure 2. Frequency distribution of $\log C_n^2$ at 5.6, 12.1, and 17.0 km, and for the median from 12 to 18 km during 11 winter months. The very low values of C_n^2 are spurious.

3. Seasonal and Interannual Variations

3.1 Mean Horizontal Winds

Figure 3 shows the mean profiles of zonal u and meridional v wind as measured by the WSMR 50-MHz radar. The number of hourly means available at 7 km is given by N on each chart. Error bars extend ± 1 standard error of the mean

(SEM) from the mean, where $SEM = 2\sigma/\sqrt{N}$ and σ is the standard deviation of the N values. The jetstream is strongest during the winter (December, January, and February), but the nose of the jet is flat. The flat nose may be understood when turbulence is very low in the center of the jet, and thus radar echoes are weak in the center of the jet and may have unacceptably low signal-to-noise values. Figure 4a compares the seasonal means of u and v . The profiles of u have a relatively similar shape. The shear of the mean wind is about the same during all seasons (except perhaps summer) in the stratosphere when discussing C_N^2 and its dependence on vertical wind shear. Profiles of the seasonal means of the absolute values of the vertical shear of zonal and meridional winds, and of the total shear, over 300-m layers based on individual profiles, are compared in figure 4b. The differences among seasons are relatively small for even these shears. In summer, the WSMR radar observations reach into the stratospheric easterlies. Meridional winds are from the south during all seasons except fall.

3.2 Mean Vertical Winds

Figure 5 shows the mean vertical velocity w and the mean of the standard deviations of vertical velocity over 1-h periods (σ_w). The mean w is downward at several centimeters to the negative first power in the troposphere, and is slightly upward in the lower stratosphere. Nastrom and VanZandt (1994) have presented a theory predicting that the observed w will be downward when there is upward energy propagation by gravity waves due to nonuniform radar reflectivities. They predict that the magnitude of w is proportional to the gravity wave amplitude. An indicator of gravity wave amplitude is σ_w . Mean profiles of w and σ_w are compared in figure 6.

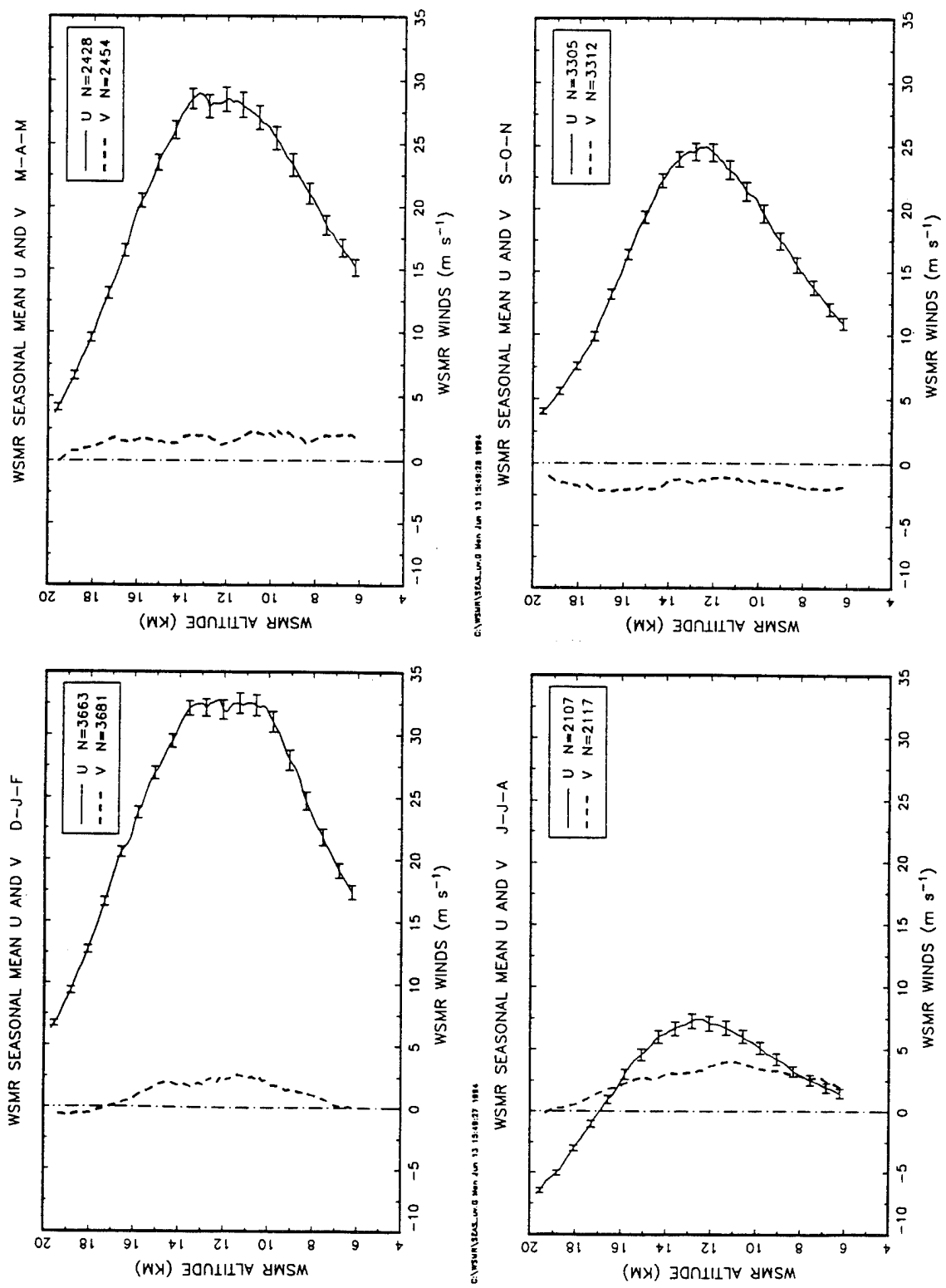


Figure 3. Seasonal mean profiles of zonal and meridional winds at WSMR.

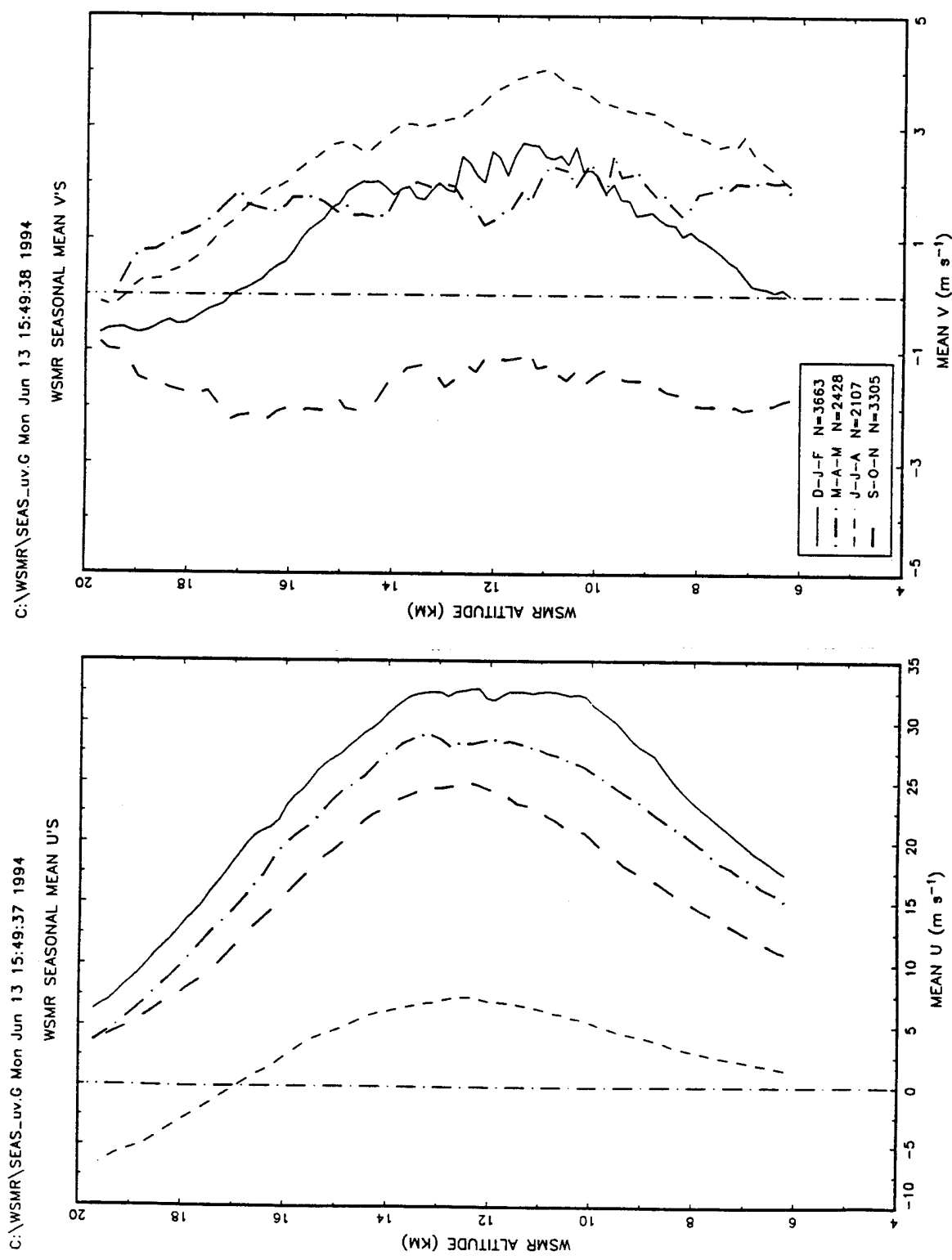


Figure 4a. Seasonal mean profiles of zonal and meridional winds at WSMR with all seasons plotted together.

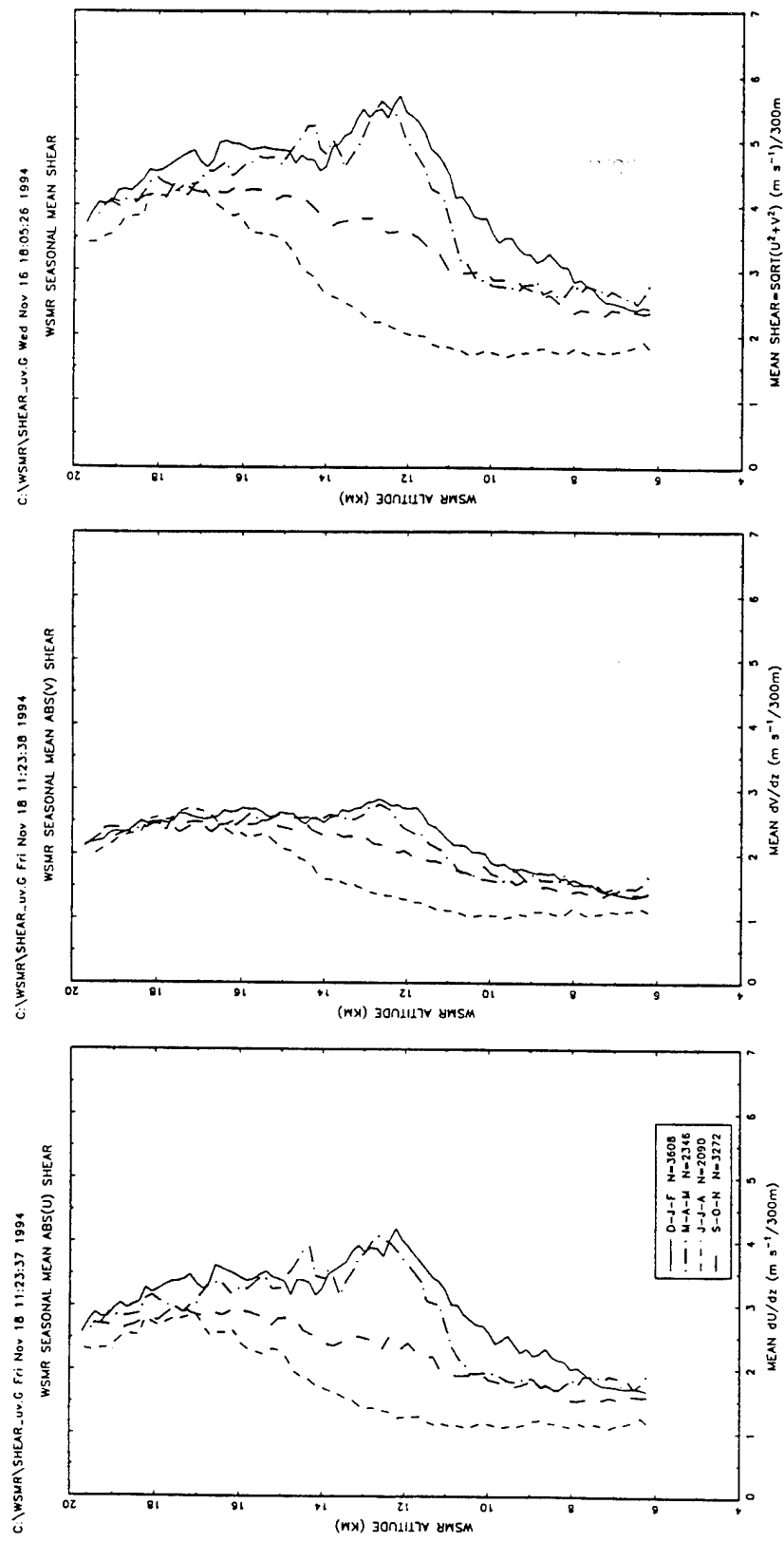


Figure 4b. Seasonal means of the vertical shear over 300-m layers of windspeed from individual observations.

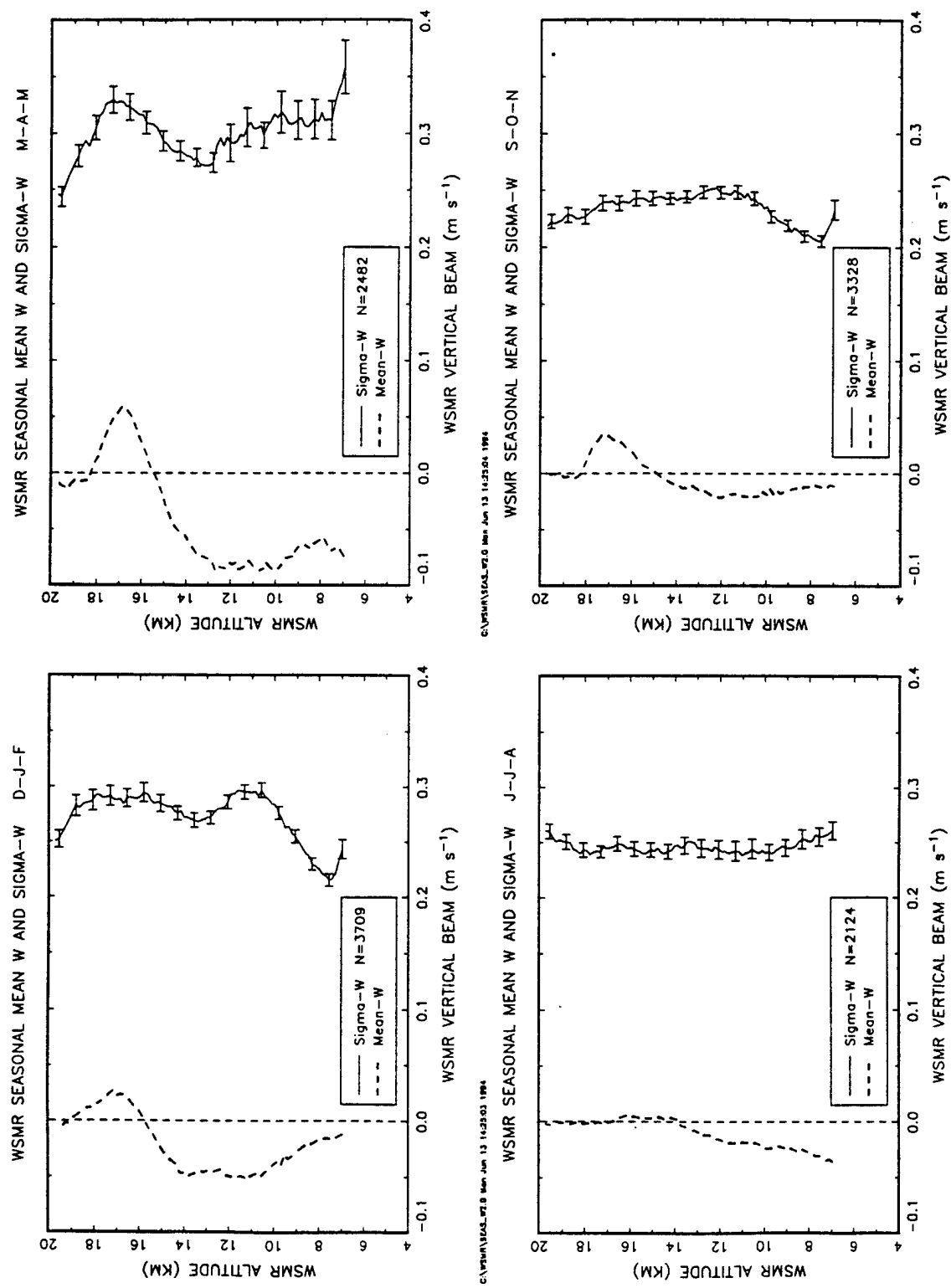


Figure 5. Seasonal mean profiles of vertical velocity and its standard deviation over 1-h periods at WSMR.
 (Note that σ_w is the standard deviation over 1 h.)

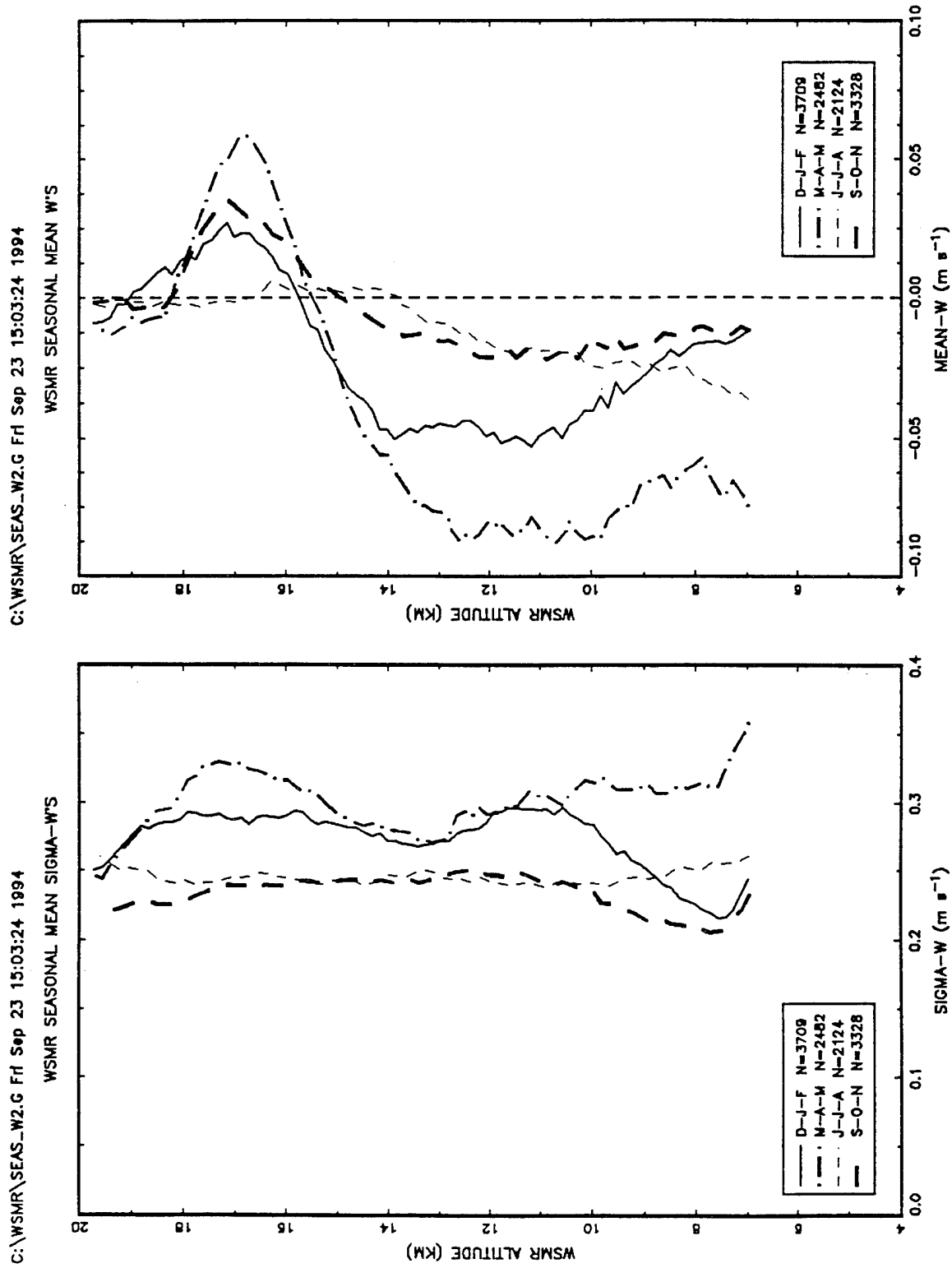


Figure 6. Seasonal mean profiles of vertical velocity and its standard deviation over 1-h periods at WSMR with all seasons plotted together.

In the troposphere, the largest w occurs during fall and winter. The largest σ_w also occurs during fall and winter, although the correlation between w and σ_w is not perfect. The correlation between w and σ_w is not perfect because trapped waves add to σ_w but make no contribution to w ; therefore, the relative proportion of trapped and propagating gravity waves may change with season.

3.3 Spectral Width

Figure 7 shows profiles of the seasonal mean spectral width along the east and north oblique beams. Spectral width is proportional to the intensity of small-scale turbulence and the eddy dissipation rate; however, as discussed by Hocking (1985) and Gage (1990), other factors such as beam broadening and vertical wind shear may contribute to the spectral width and must be accounted for before using width as a turbulence variable. The spectral width from the vertical beam is not used at very high frequency because echoes from both turbulence and specular reflections are expected. In figure 7, note that the width of the meridional beam is greater during all seasons except summer, and that the difference between beams is usually greatest in the troposphere. Figure 8 compares the seasonal means from the zonal beam; the greatest widths are seen during winter and spring. In the troposphere below approximately 7 km, there is little variation with season.

3.4 C_N^2

Figure 9 shows profiles of the seasonal mean of $\log C_N^2$ (because the logarithm of C_N^2 is normally distributed, its use permits routine statistical procedures) and compares the zonal and meridional beams. As with width, the value of the meridional beam is greater during all seasons; however, for C_N^2 the difference is greatest in the stratosphere and seems to be approximately the same magnitude during every season. Figure 10 (right-hand panel) compares the annual mean profiles for the two beams; the zonal beam's values are smaller: about 1 dB in the troposphere and 2 dB in the stratosphere. The vertical shapes of the mean profiles resemble the shape of the vertical profile of the potential refractivity, M^2 . M^2 is proportional to the humidity, the vertical gradient of humidity, and the vertical gradient of temperature as well as the density of air.

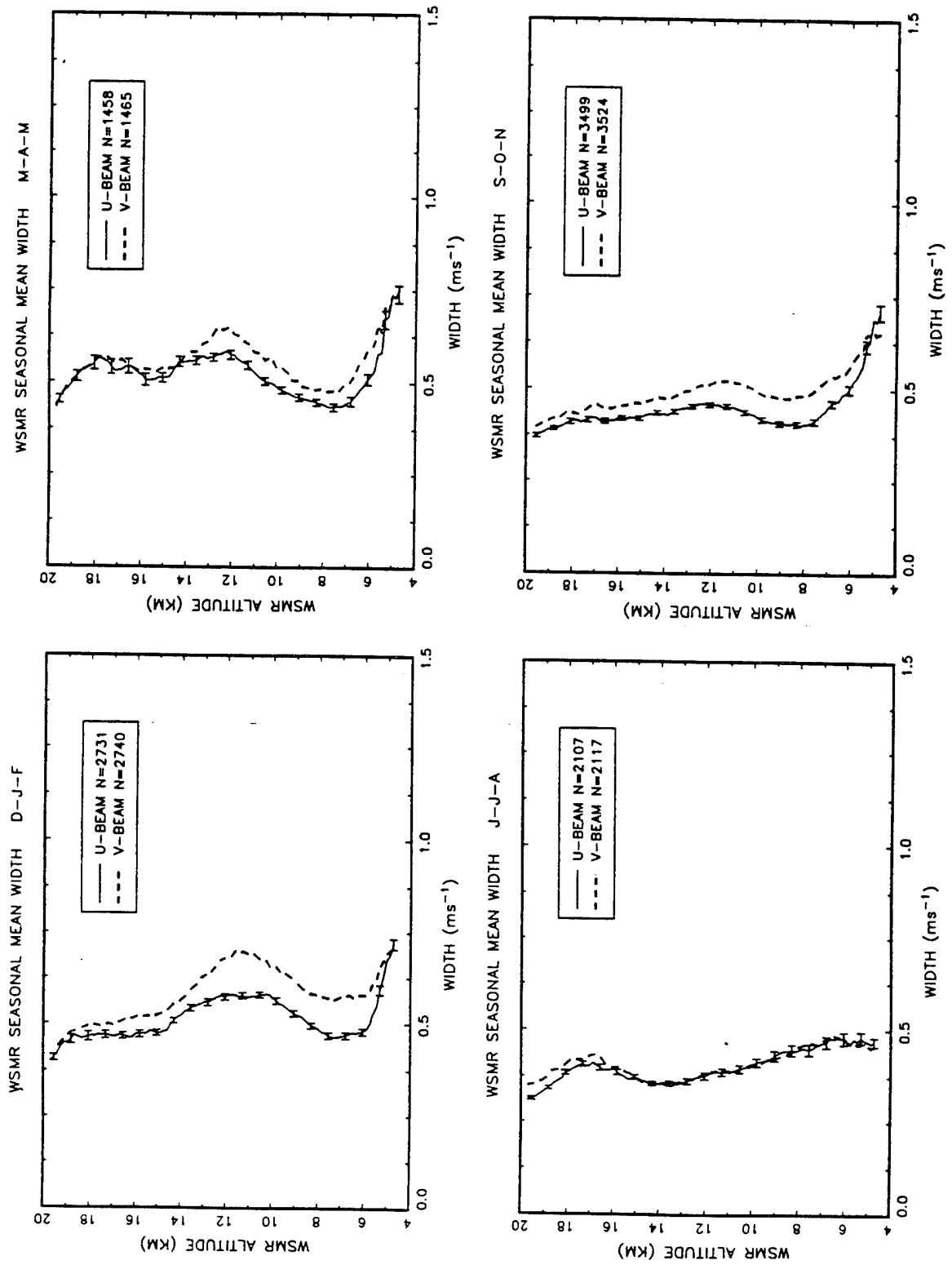


Figure 7. Seasonal mean profiles of spectral width at WSMR.

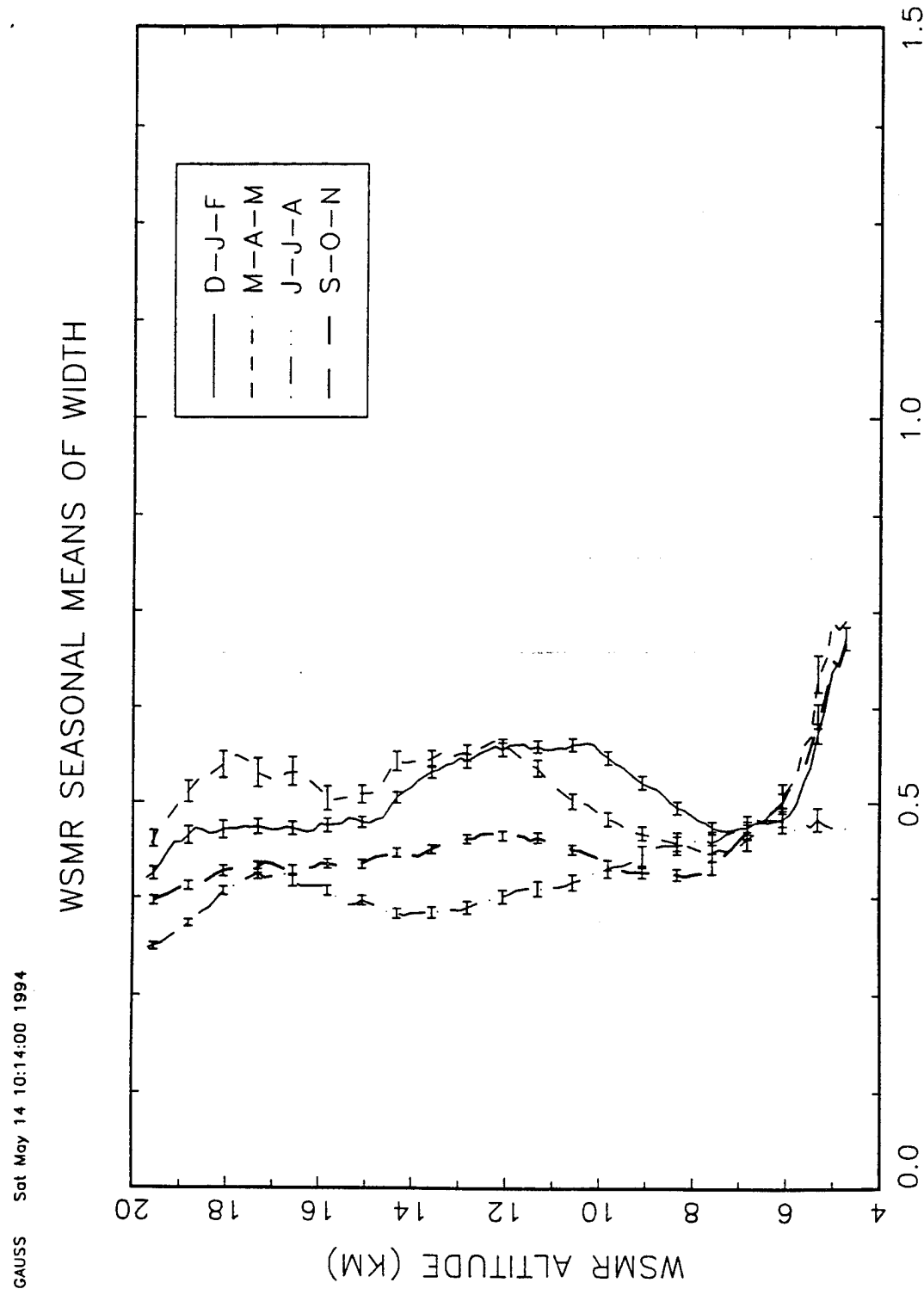


Figure 8. Seasonal mean profiles of spectral width at WSMR with all seasons plotted together.

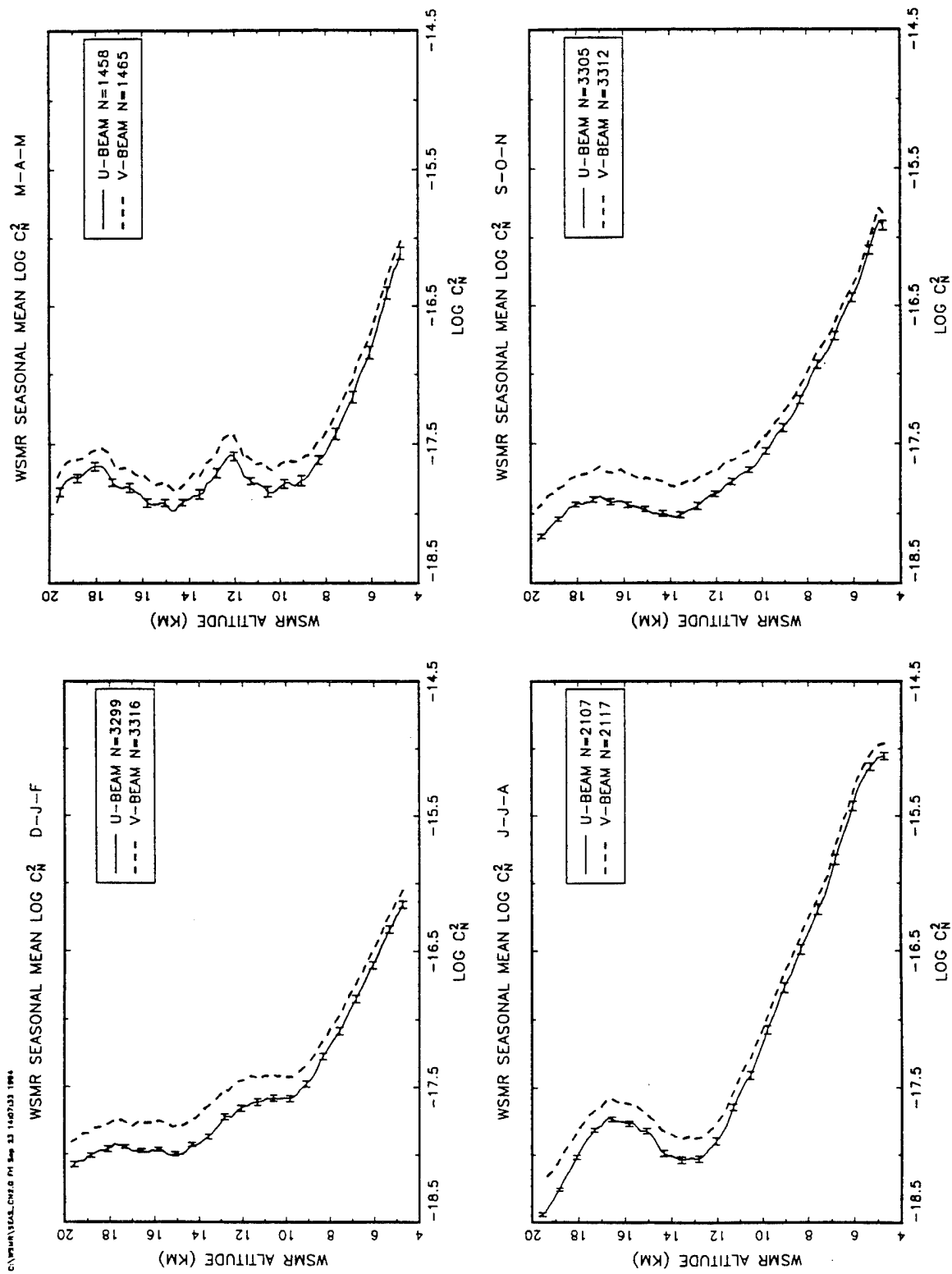


Figure 9. Seasonal mean profiles of $\log C_N^2$ at WSMR.

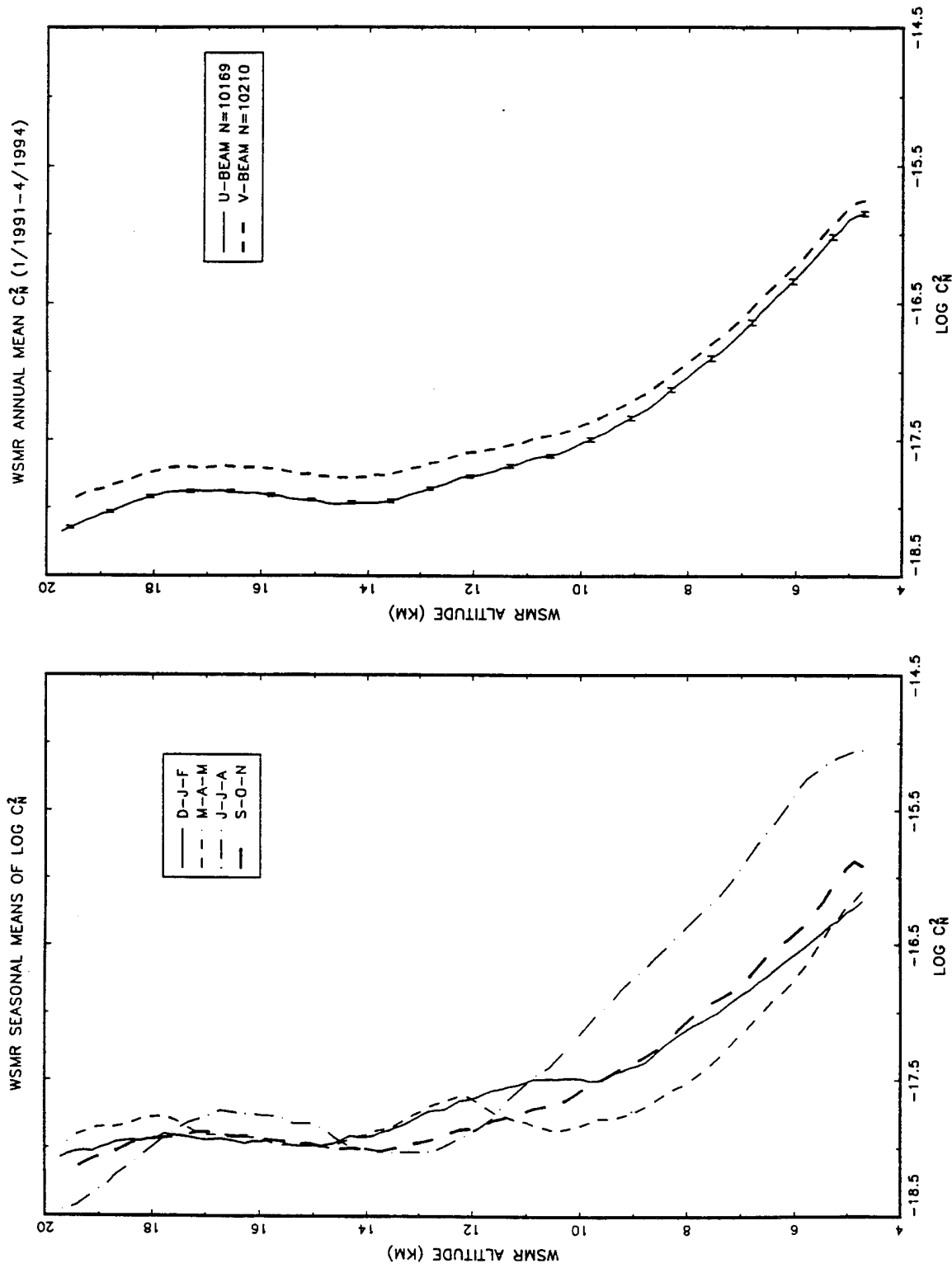


Figure 10. Annual mean of $\log C_N^2$ (right side) and seasonal means of $\log C_N^2$ (left side).

Local values of C_N^2 are given by

$$C_N^2 = \alpha^2 \alpha' L_0^{4/3} M^2 \quad (1)$$

where

- α = a constant close to unity
- α' = the ratio of the eddy diffusivities and is near unity
- L_0 = the outer scale of turbulence.

M^2 is given by

$$M^2 = (77 * 10^{-6} \frac{P}{T\theta})^2 \left\{ \frac{\delta \theta}{\delta z} \left(1 + \frac{15500q}{T} \right) - \frac{15500q}{2T} \frac{\delta q}{\delta z} \right\}^2 \quad (2)$$

where the symbols have their usual meanings (Gage 1990). Mean values of C_N^2 as seen by the radar depend on the fraction of the sample volume that is actively turbulent.

Variations with season of C_N^2 are compared in figure 10 (left-hand panel). Largest values of $\log C_N^2$ are in the troposphere during summer due to increased humidity. In the troposphere, the single largest contribution to the variability of M^2 comes from humidity gradients (Gage 1990; Tsuda et al. 1988). During the other seasons and in the stratosphere, there is surprisingly relatively little variation of $\log C_N^2$. The stratospheric static stability does not change much with season and, as seen in figure 4, the mean wind shear (leading to local turbulence) is also fairly constant with season.

Profiles of the standard deviation of $\log C_N^2$ are given in figure 11. The curves labeled HOURLY are the standard deviation of the N hourly mean values of $\log C_N^2$ available during a season. The hourly curves depict the low-frequency variations of $\log C_N^2$ and contain the variance due to processes such as year-to-year changes and diurnal changes. The curves labeled HI FREQ are the averages of the standard deviations of $\log C_N^2$ within each hour. There are usually 20 individual observations taken in an hour. Note that there is very little change among seasons of the high-frequency variations.

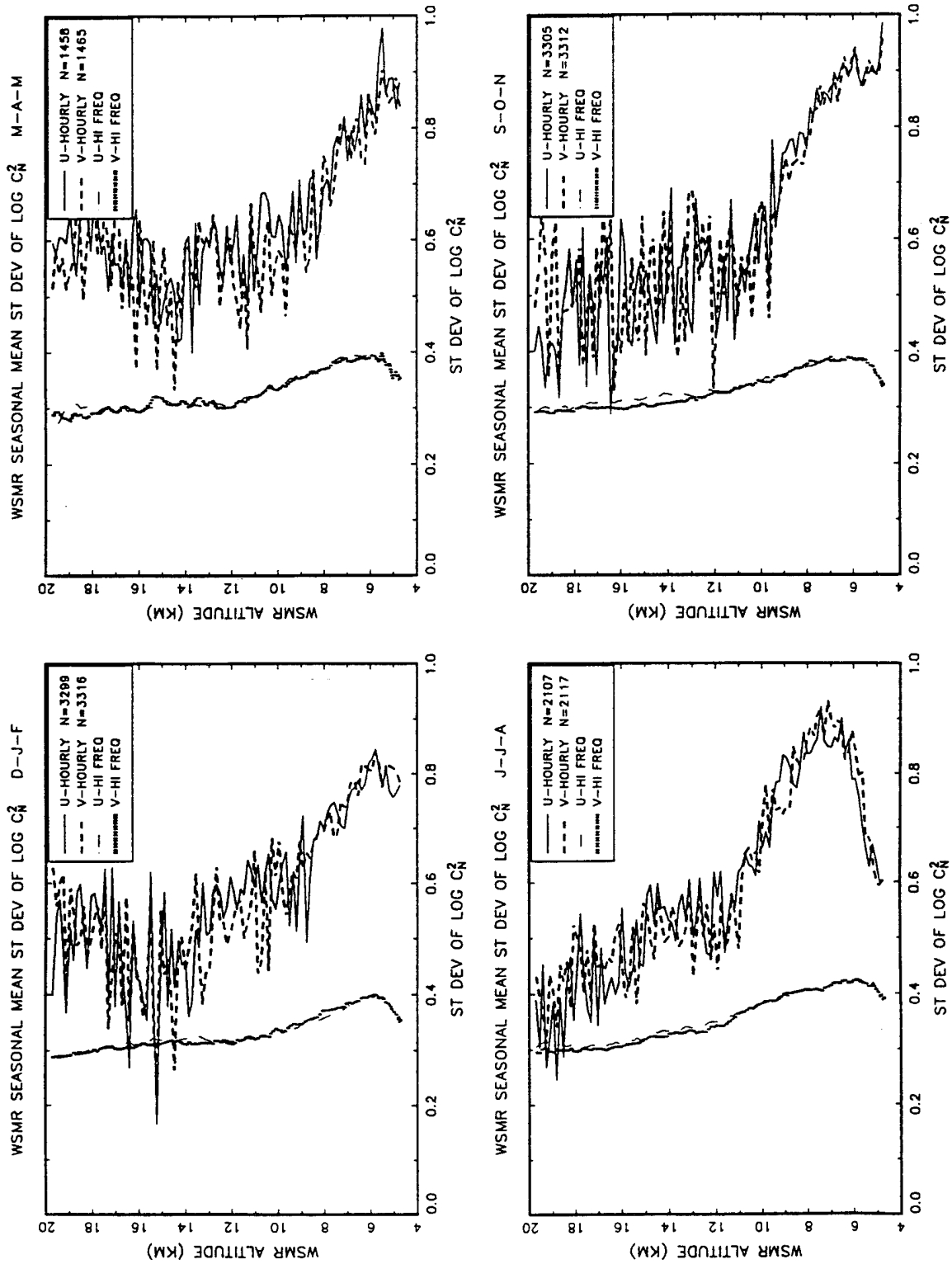


Figure 11. Seasonal mean profiles of standard deviation of $\log C_N^2$ (Hourly) and of standard deviation of $\log C_N^2$ over 1 h (Hi Freq) at WSMR.

$\log C_N^2$ is relatively constant with height in the stratosphere in figures 9 and 10 and knowing the median value (for a normal distribution, the mean and the median are equivalent; using median values ensures that results are not distorted by an unusual outlier) between 12 and 18 km would provide a great deal of information on the profile. Therefore, the median value between 12 and 18 km was included in figure 1 in the frequency distributions during winter. Frequency distributions of $\log C_N^2$ at 5.1, 12.1, and 17.0 km, and for the median from 12 to 18 km during the other seasons are given in figures 12 through 14. During all seasons, the distributions are broadest at 5.6 km.

Interannual variations of the seasonal means of $\log C_N^2$ are given in figure 15. The interseasonal variations seen in figure 10 and again in figure 15 are clearly much more important than the interannual variations seen for any given season in figure 15, because every year the mean summer profiles in the troposphere are the largest and values for spring and winter are the smallest. Variations are relatively small in the stratosphere. There is no apparent trend of C_N^2 with time at any height at WSMR, in contrast to the year-to-year trend in CO reported by Frisch et al. (1990).

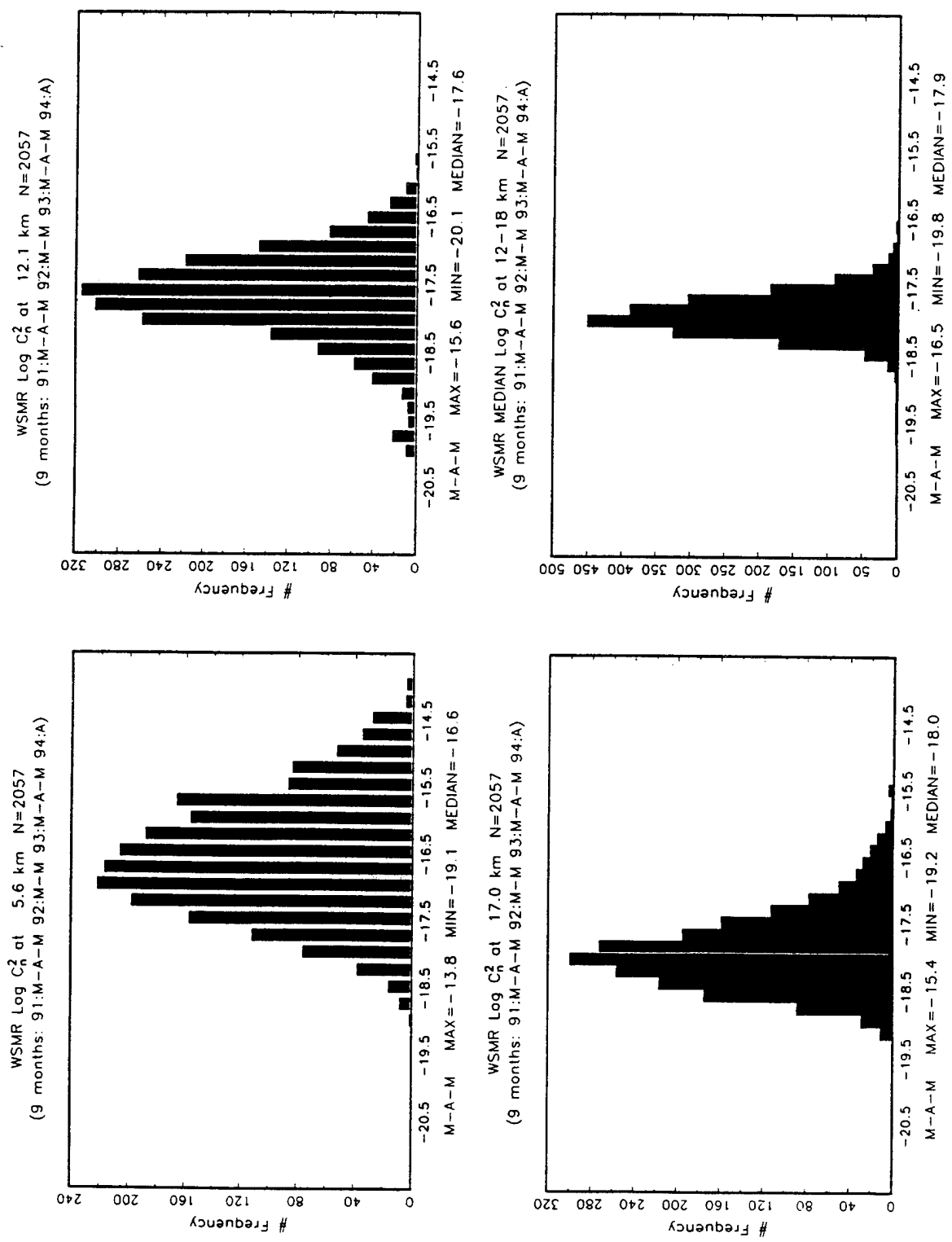
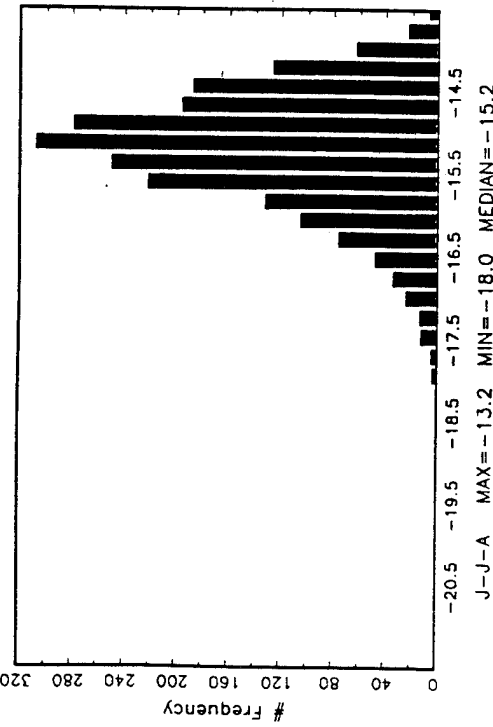
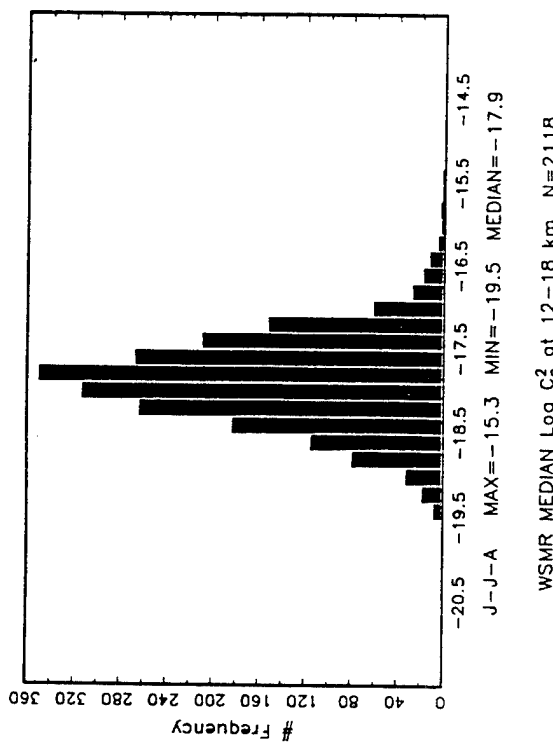


Figure 12. Frequency distribution of $\log C_n^2$ at 5.6, 12.1, and 17.0 km, and for the median from 12 to 18 km during 9 spring months.

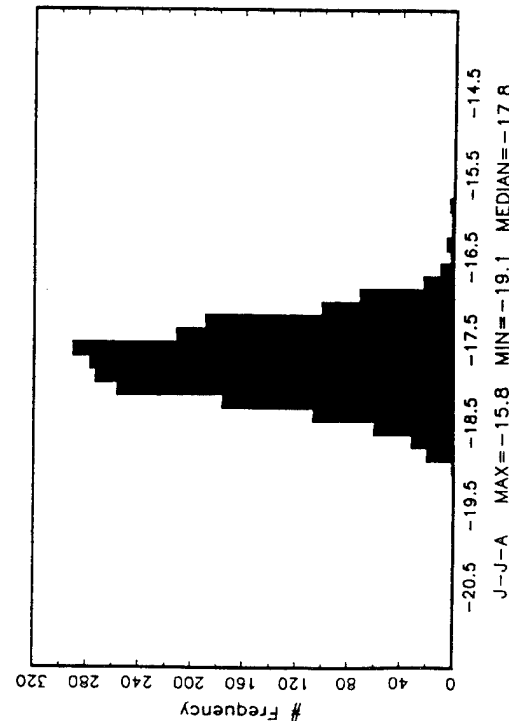
WSMR Log C_n^2 at 5.6 km N=2118
(8 months: 91:J-J-A 92:J-J-A 93:J-A)



WSMR Log C_n^2 at 12.1 km N=2118



WSMR Log C_n^2 at 17.0 km N=2118



WSMR Log C_n^2 at 12.1 km N=2118

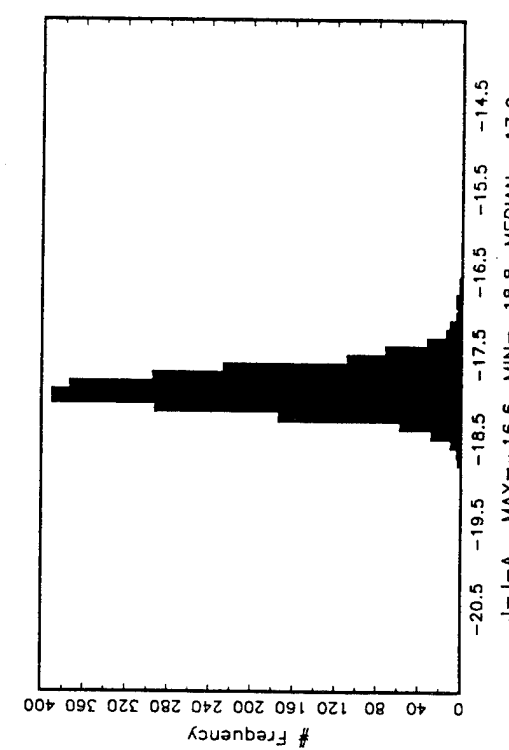


Figure 13. Frequency distribution of $\log C_n^2$ at 5.6, 12.1, and 17.0 km, and for the median from 12 to 18 km during 8 summer months.

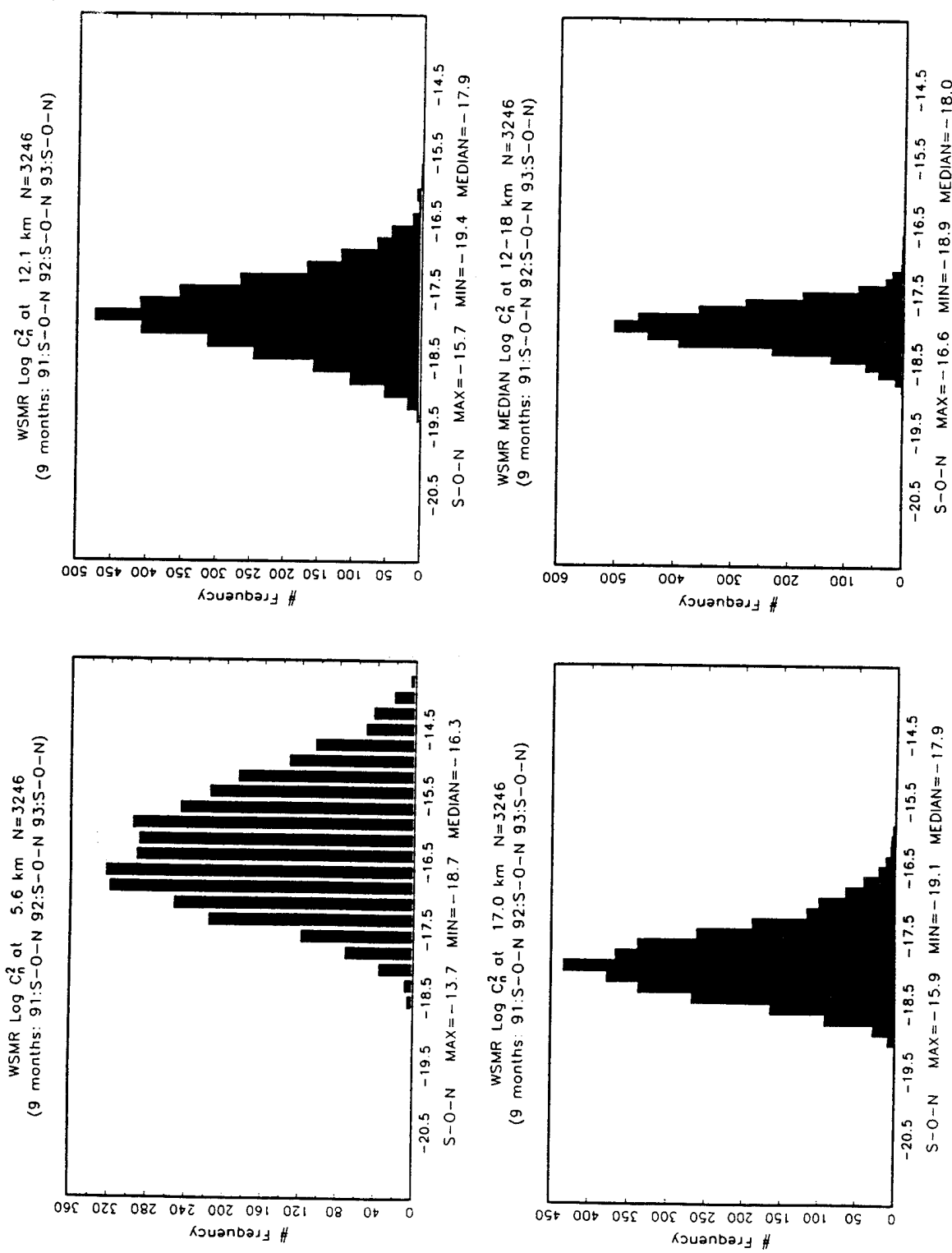


Figure 14. Frequency distribution of $\log C_n^2$ at 5.6, 12.1, and 17.0 km, and for the median from 12 to 18 km during 9 fall months.

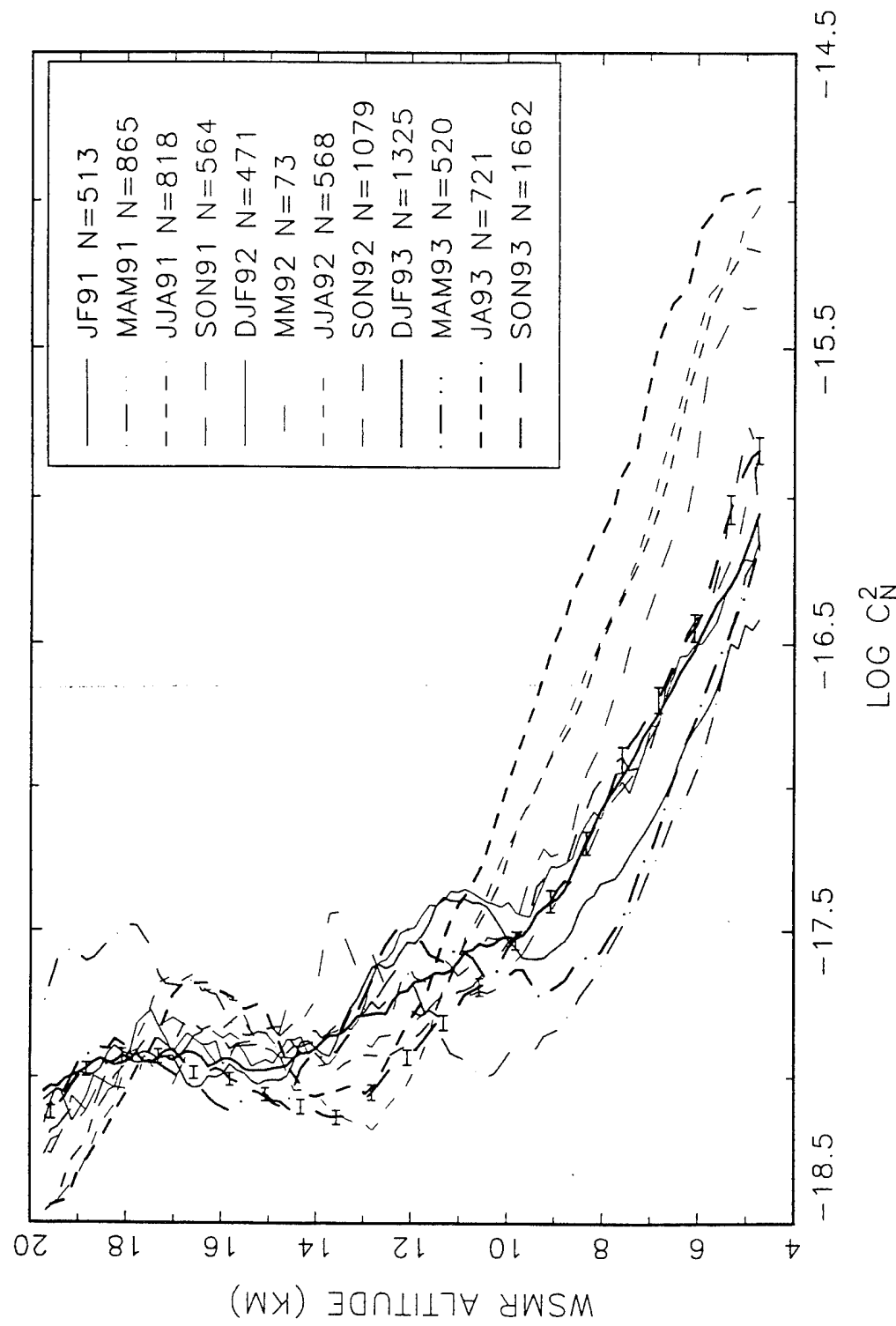
WSMR SEASONAL MEANS OF $\log C_N^2$ 1991-1993

Figure 15. Comparison of individual seasonal means to show interannual variations of $\log C_N^2$.

4. Autocorrelation of Log C_N^2

The autocorrelation functions of $\log C_N^2$ at 7, 12, and 17 km for each of the three radar beams are given in figures 16, 17, and 18 for January, February, and July 1993, respectively. The left-hand panels show the autocorrelation functions from lag 0 to about lag 300 min (5 h); also given are the number of data pairs at lags 0, 3, and 6 min. The right-hand panel shows the segment of the data from the left-hand panel for lags out to 27 min in semilogarithmic coordinates. These results suggest the autocorrelation function $r(\tau)$ can be modeled fairly well as the sum of a first-order autoregressive process and a random process; that is,

$$r(\tau) = a e^{-\nu\tau} \quad (3)$$

where $a < 1$ and $\nu < 0$. The quantity a reflects the random process. The decay rate of the red-noise process is ν . Taking the logarithm of equation (3) gives

$$\ln r(\tau) = \ln a + \nu\tau \quad (4)$$

which shows this model will be linear in semilogarithmic coordinates. Some of the curves in the right-hand panels of figures 16 through 18 appear to decrease rapidly from lag 3 min to lag 6 min and then decrease linearly at higher lags. This shape implies there is also a small contribution to the autocorrelation function from a moving-average process, quite likely due to blobs of turbulence that overlap from one observation to the next. Surprisingly, there is little apparent difference in the autocorrelation functions between the troposphere and stratosphere. Past reports of persistent layers in the stratosphere as reviewed by Gage (1990) might have led one to expect larger autocorrelation values in the stratosphere. A study of persistent layers at WSMR is currently being conducted.

Using equation (4), the autocorrelation function can be integrated to estimate the effective time T between independent observations using the relation

$$T = 2 \int_0^\infty r(\tau) d\tau. \quad (5)$$

The curves in figures 16 through 18 suggest v is about $7.1 \times 10^{-3} \text{ min}^{-1}$, and that $0.5 < \alpha < 0.9$. T ranges from approximately 2 to 4 h with these values. This is the average time between statistically independent observations when employing these estimates. The time before another observation is needed may be much shorter for a particular situation or application.

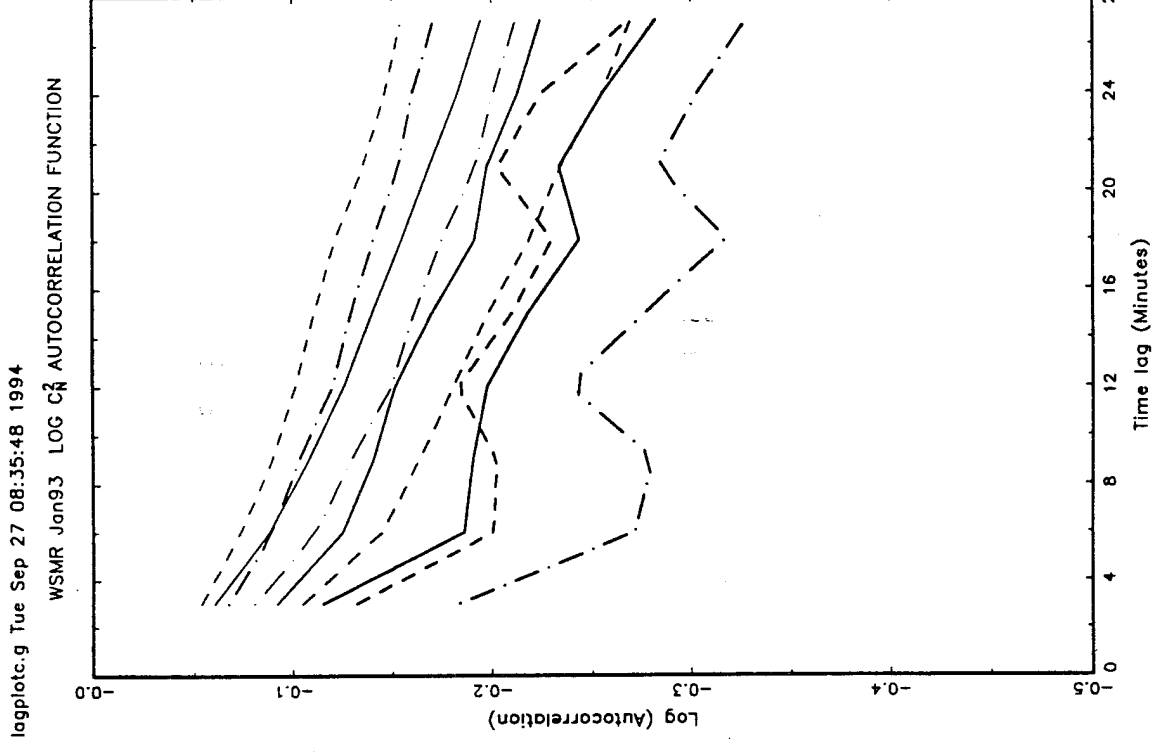
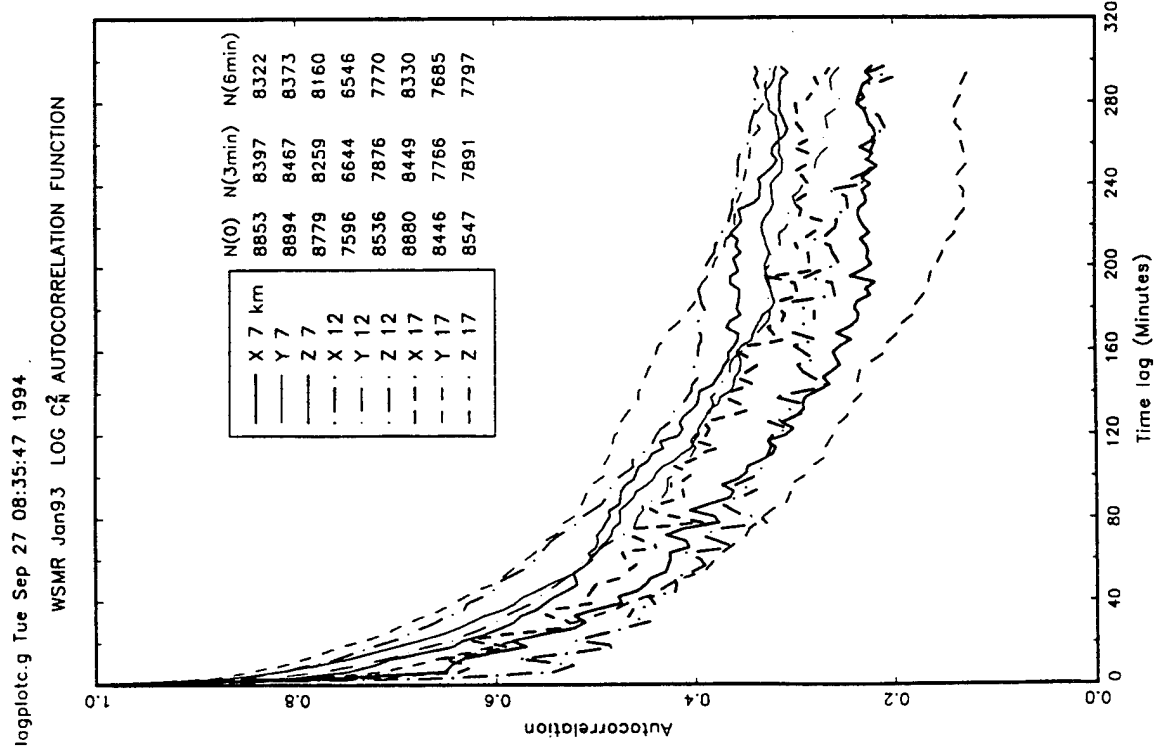


Figure 16. Autocorrelation function of individual observations of $\log C_n^2$ during January 1993 out to lag 300 min (left side). The right side is out to lag 27 min and in semilogarithmic coordinates.

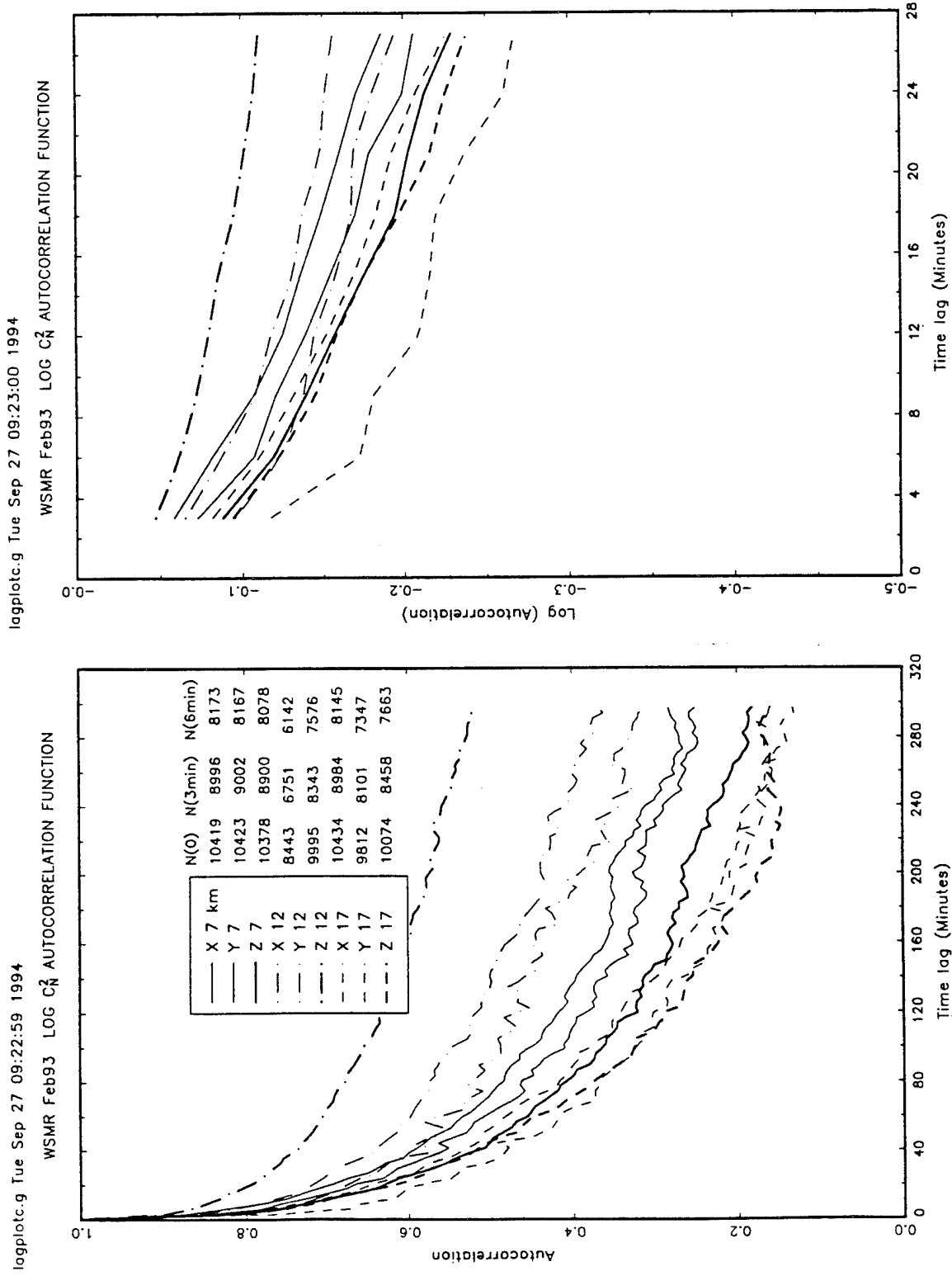


Figure 17. Autocorrelation function of individual observations of $\log C_N^2$ during February 1993 out to lag 300 min (left side). The right side is out to lag 27 min and in semilogarithmic coordinates.

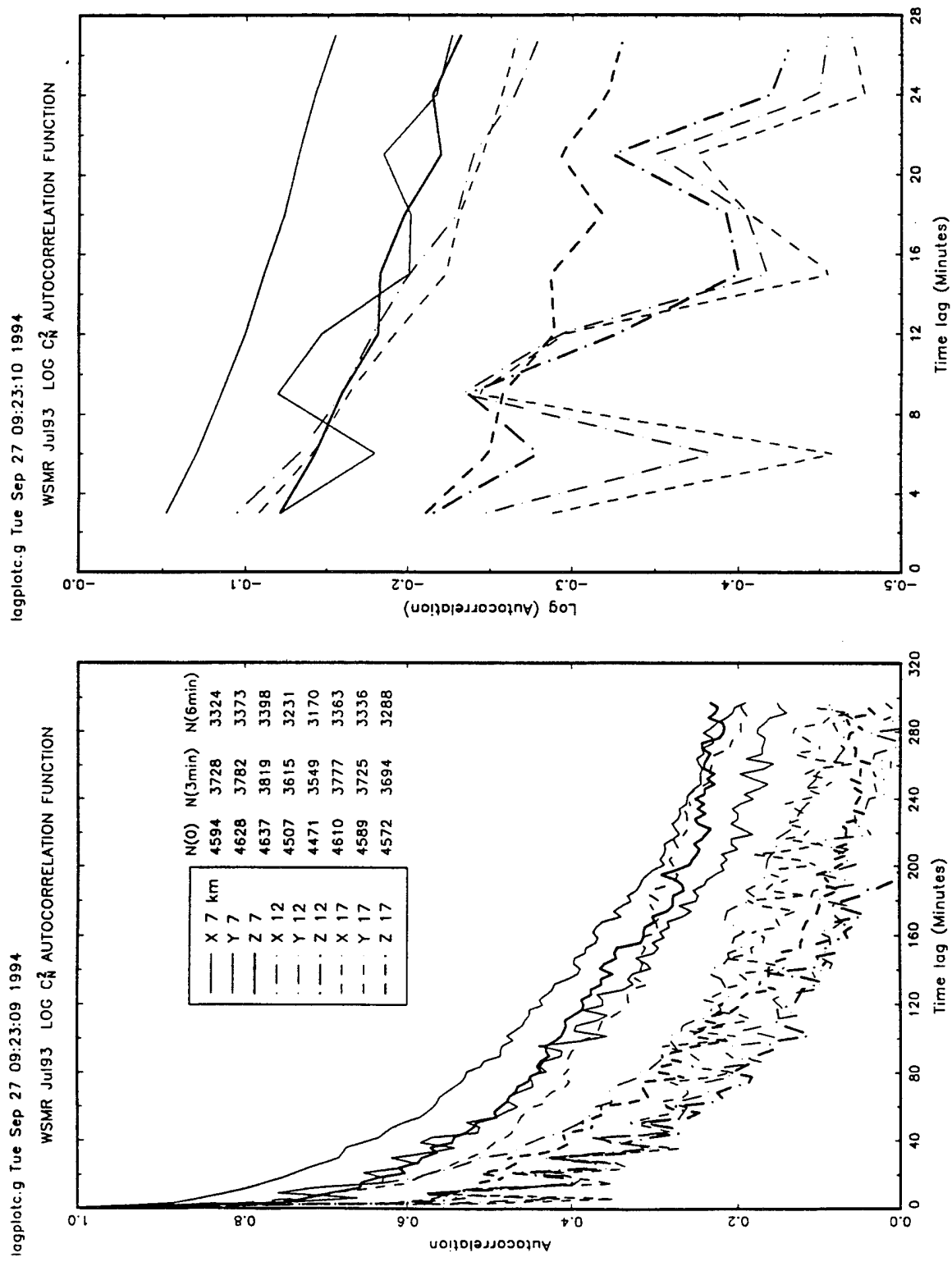


Figure 18. Autocorrelation function of individual observations of $\log C_N^2$ during July 1993 out to lag 300 min (left side). The right side is out to lag 27 min and in semilogarithmic coordinates.

5. Diurnal Variations

To study diurnal changes in $\log C_N^2$, windspeed, and spectral width, the data were sorted according to hour of the day during each season. Time series of the 24-h means were inspected for apparent diurnal cycles. For example, figures 19 through 22 show the diurnal curves for beam 2 (the meridional plane) during each season. In each chart, seven range gates have been averaged to give curves for layers 1.05 km deep for speed, width, and $\log C_N^2$. In the lower right panel of each chart, 20 range gates have been averaged for $\log C_N^2$ to give layers 3 km deep. There is an apparent semidiurnal variation in speed in the lower stratosphere, becoming more nearly diurnal at the upper levels shown, especially during the fall through the spring. Width and $\log C_N^2$ have only small diurnal changes above the midtroposphere during all seasons. Width has a large afternoon maximum in the troposphere, especially during the summer.

The hourly standard deviation of vertical velocity σ_w has a relatively large diurnal variation. Figures 23 through 26 show the diurnal curves of σ_w over layers 1.05 and 3 km deep from 7.7 to 19.3 km in the lower panels. Largest values of σ_w tend to be found in the afternoon, near 22 UTC. The upper panels show w and width. There does not appear to be a large change of the diurnal cycle in σ_w with altitude. (The spikes of σ_w seen at 16 and 20 UTC during spring are clearly anomalous.) No pattern of diurnal cycle in w can be seen except in the troposphere during spring. Figure 27 shows the hourly vertical profiles of σ_w for each season. Clearly, the general form of the diurnal variation in σ_w does not change much with height in a given season. The diurnal range is largest during summer. Sato (1990, 1992) has discussed the diurnal changes in vertical wind variability at the MU radar in Japan.

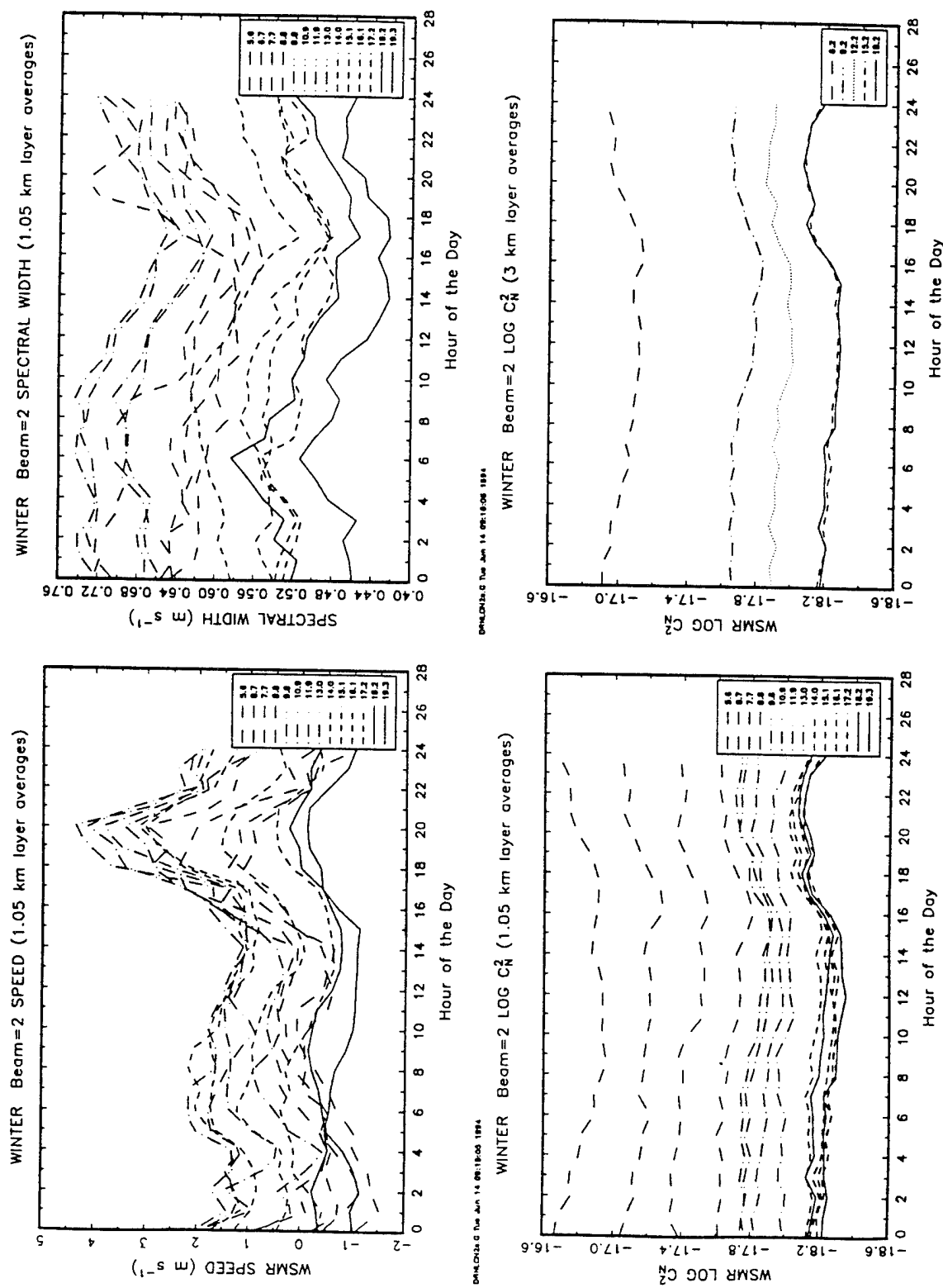


Figure 19. Diurnal variations of windspeed, spectral width, and $\log C_N^2$ during winter on the beam in the meridional plane.

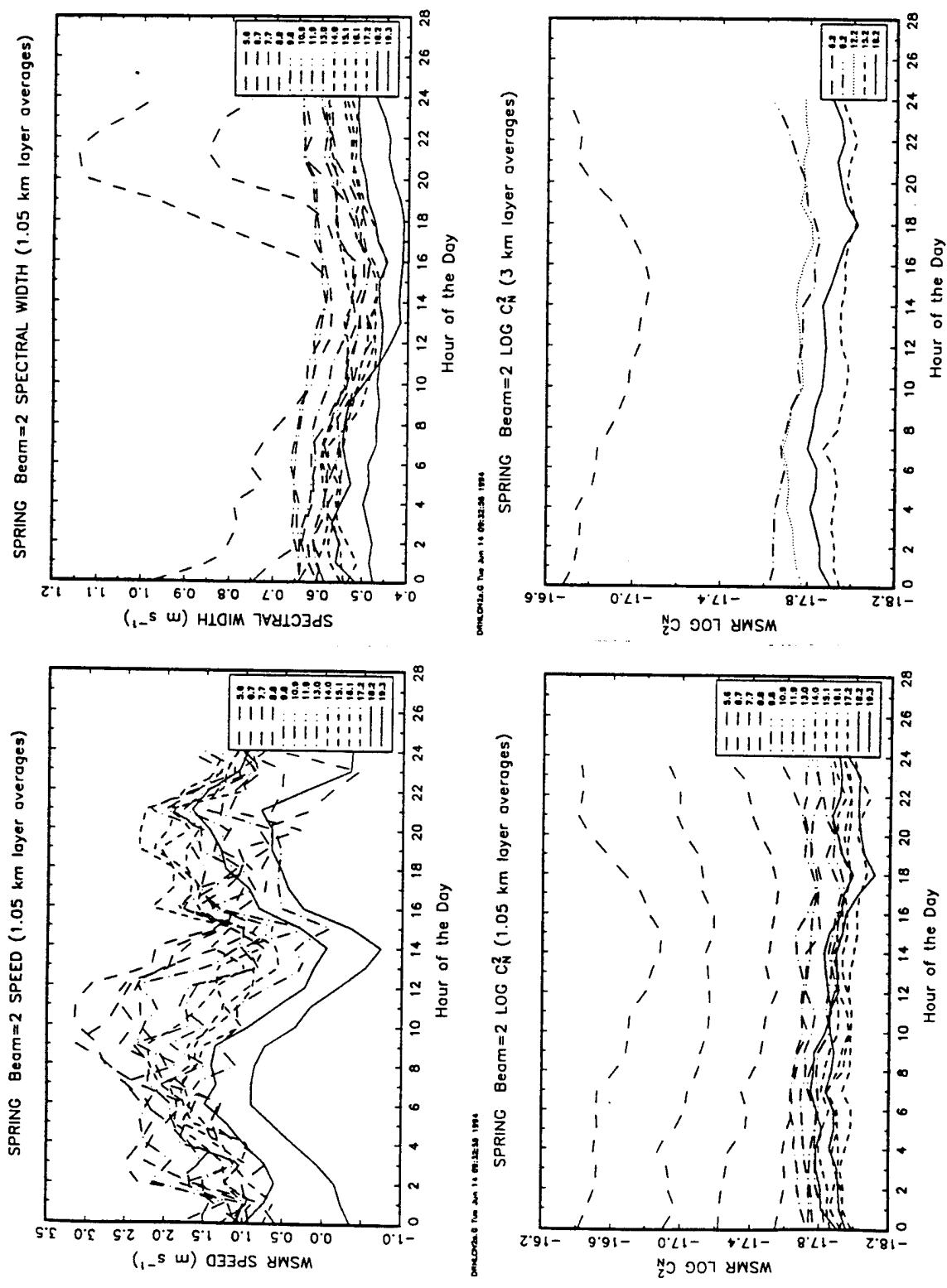


Figure 20. Diurnal variations of windspeed, spectral width, and $\log C_N^2$ during spring on the beam in the meridional plane.

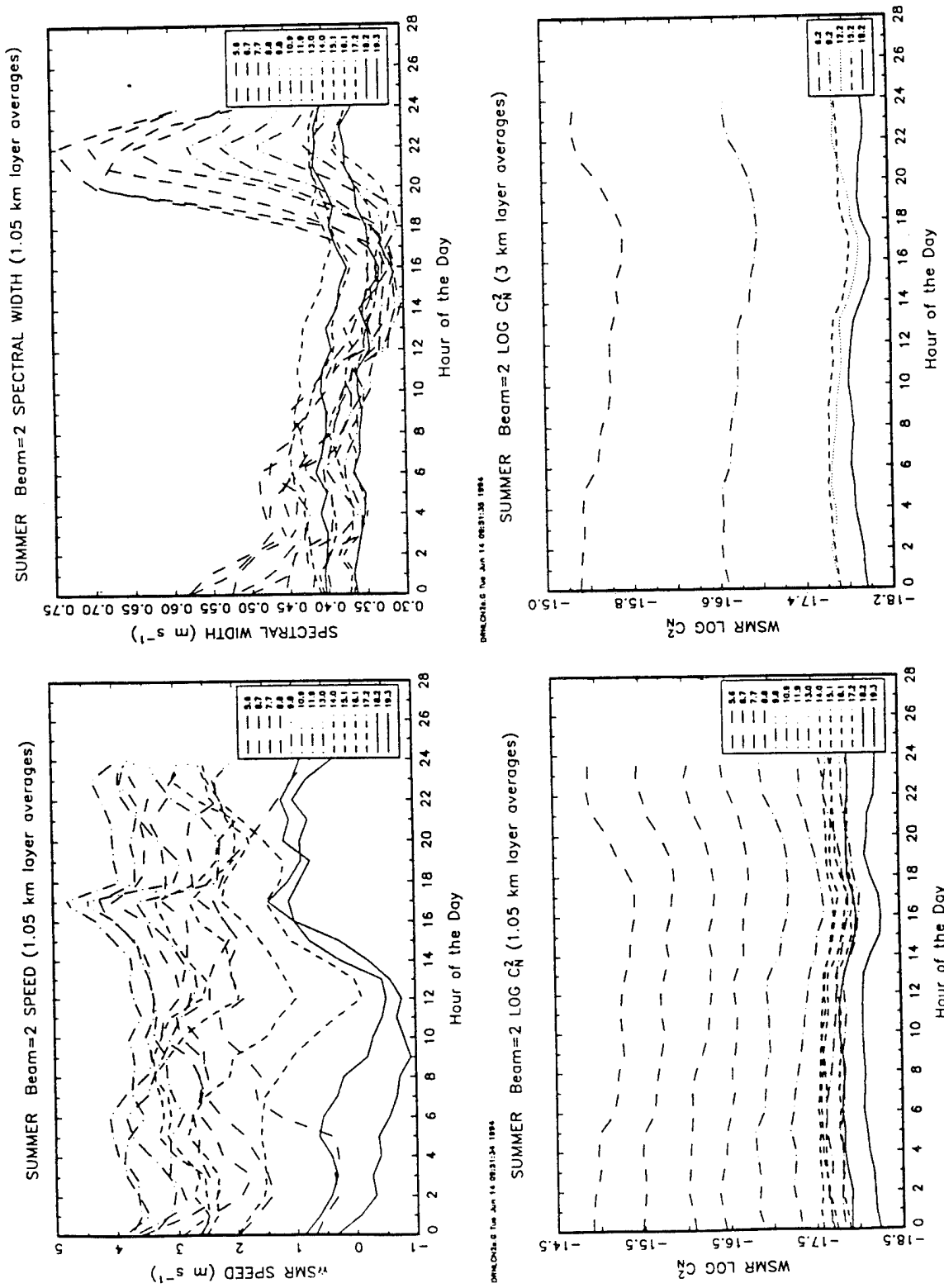


Figure 21. Diurnal variations of windspeed, spectral width, and $\log C_N^2$ during summer on the beam in the meridional plane.

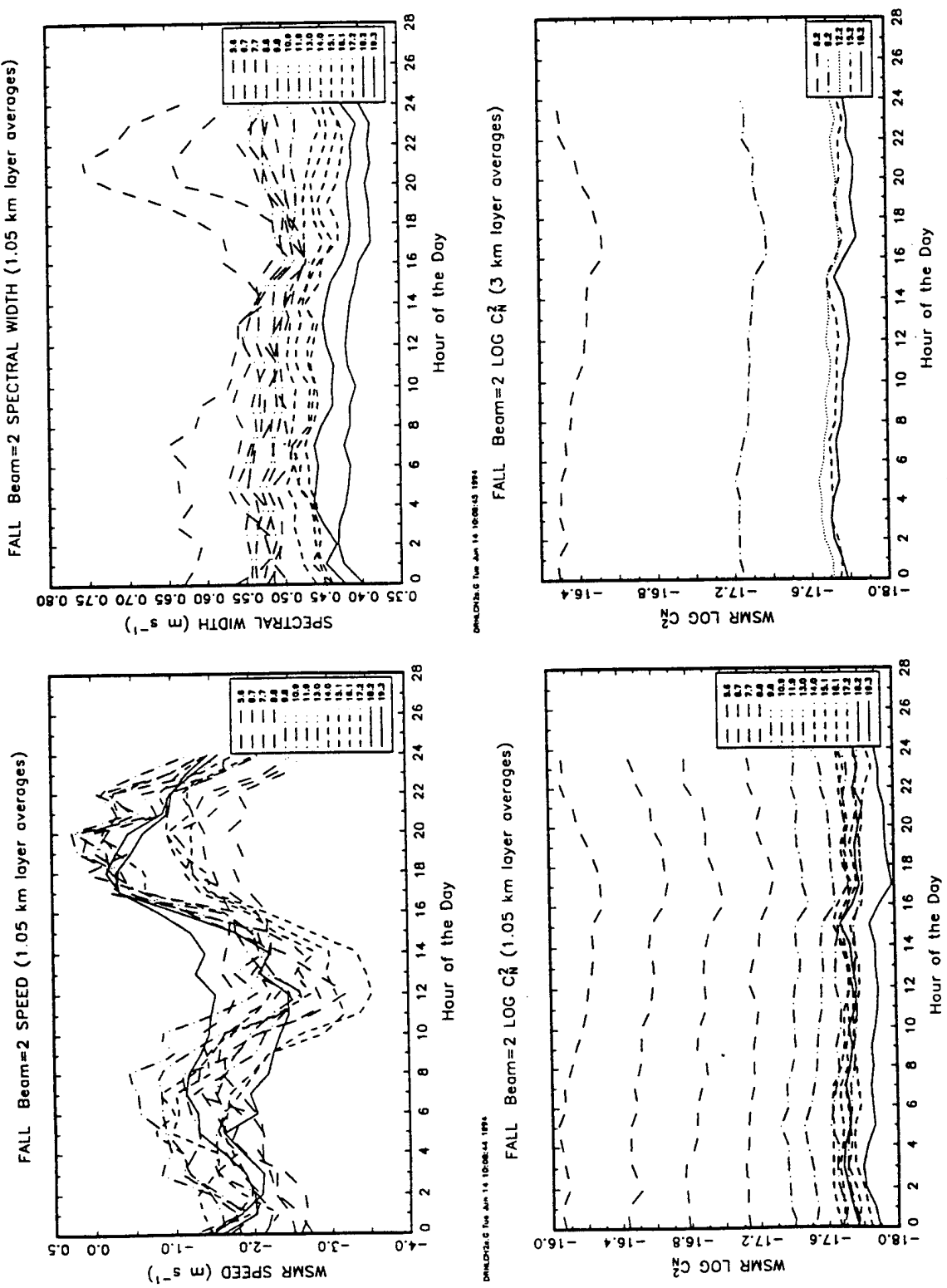


Figure 22. Diurnal variations of windspeed, spectral width, and $\log C_n^2$ during fall on the beam in the meridional plane.

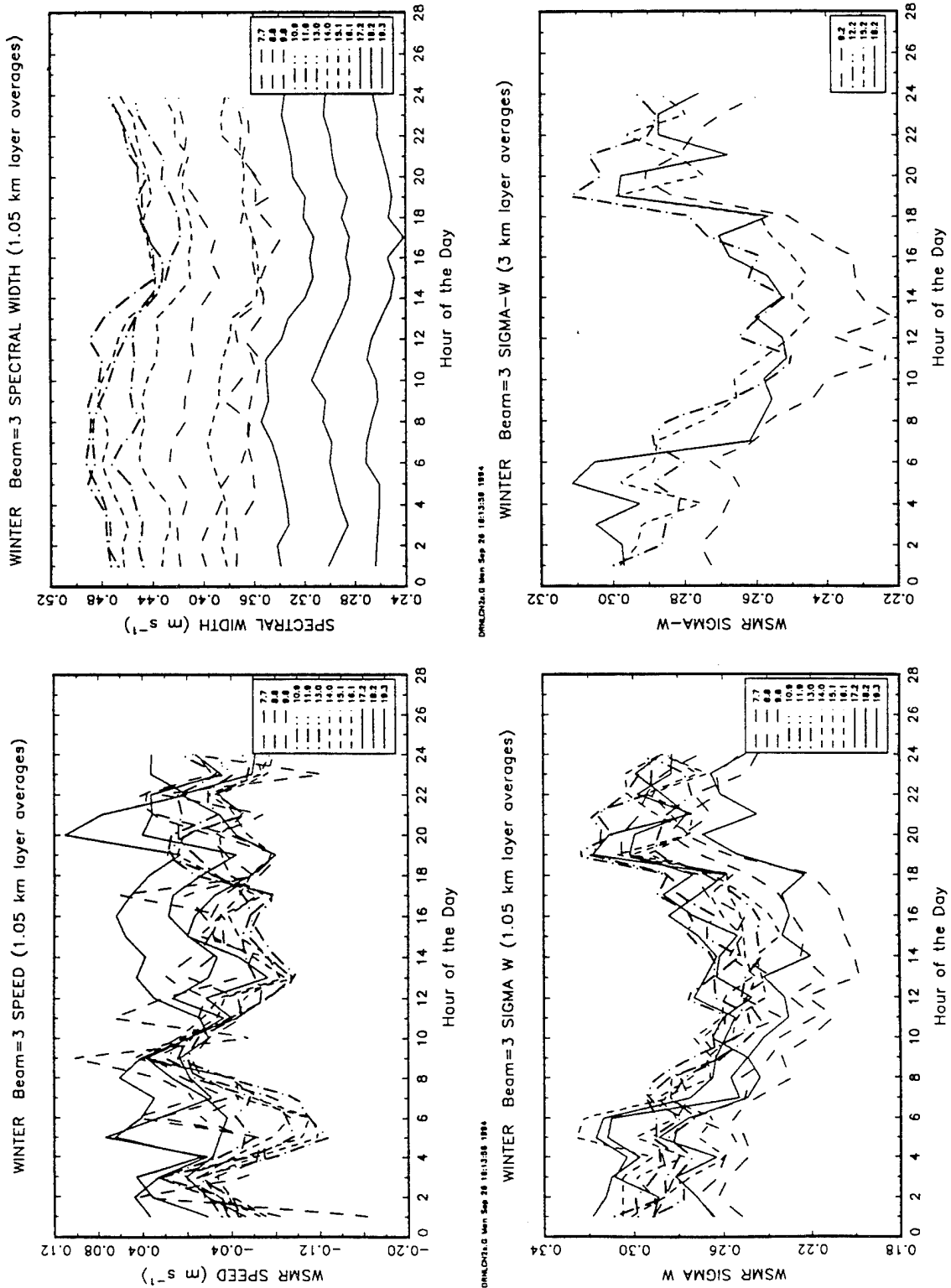


Figure 23. Diurnal variations of windspeed, spectral width, and σ_w during winter on the beam in the meridional plane.

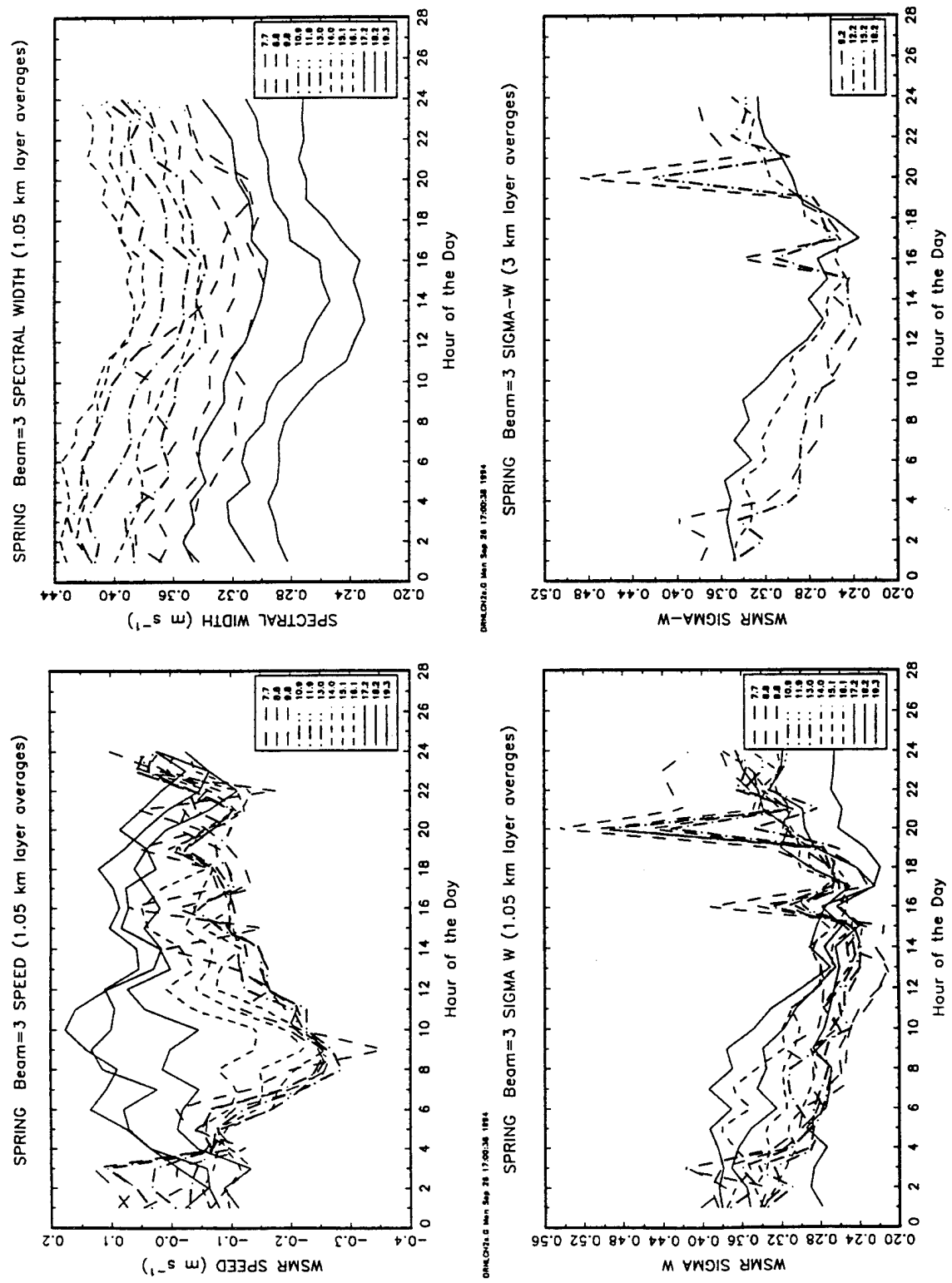


Figure 24. Diurnal variations of windspeed, spectral width, and σ_w during spring on the beam in the meridional plane.

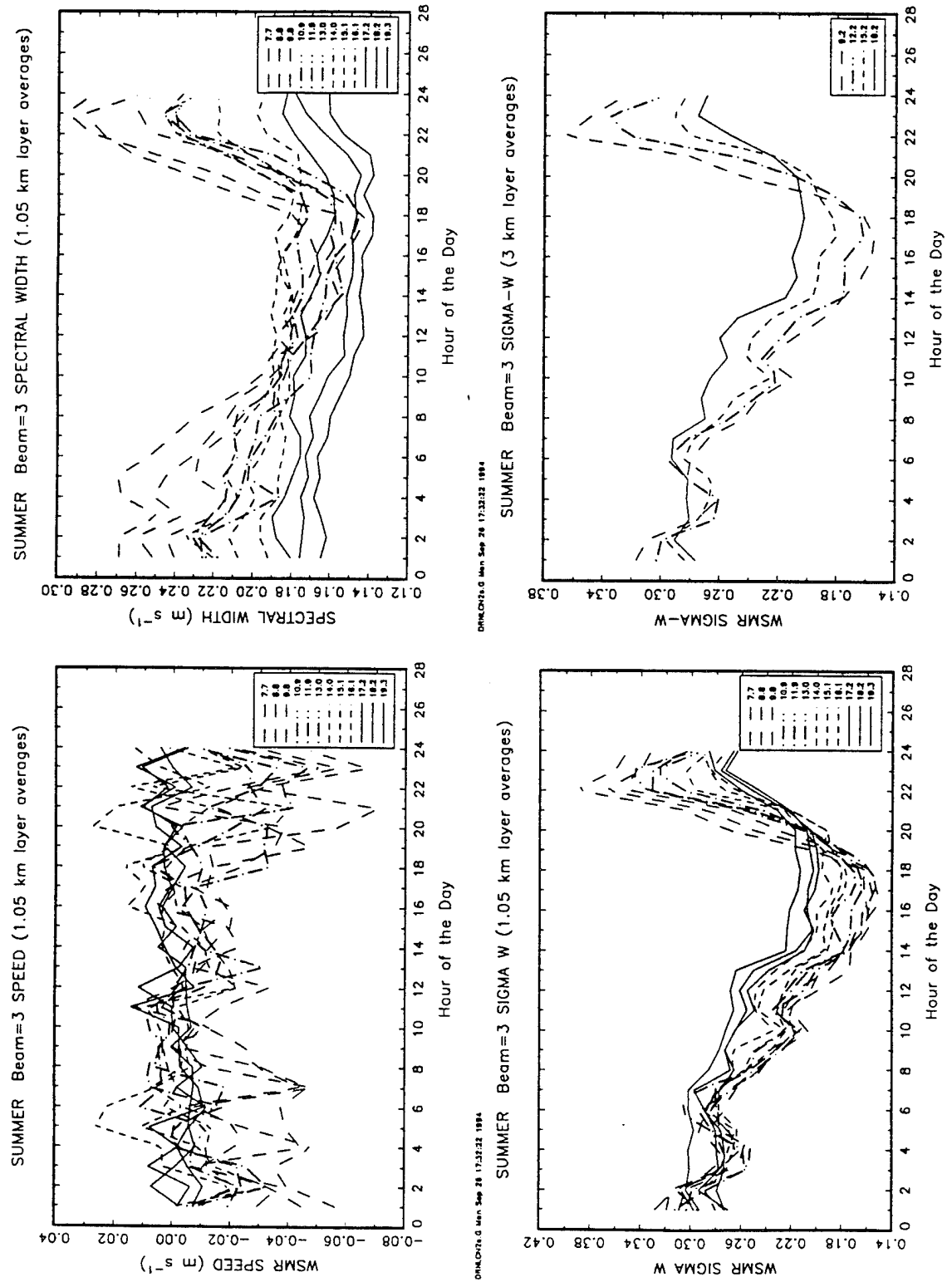


Figure 25. Diurnal variations of windspeed, spectral width, and σ_w during summer on the beam in the meridional plane.

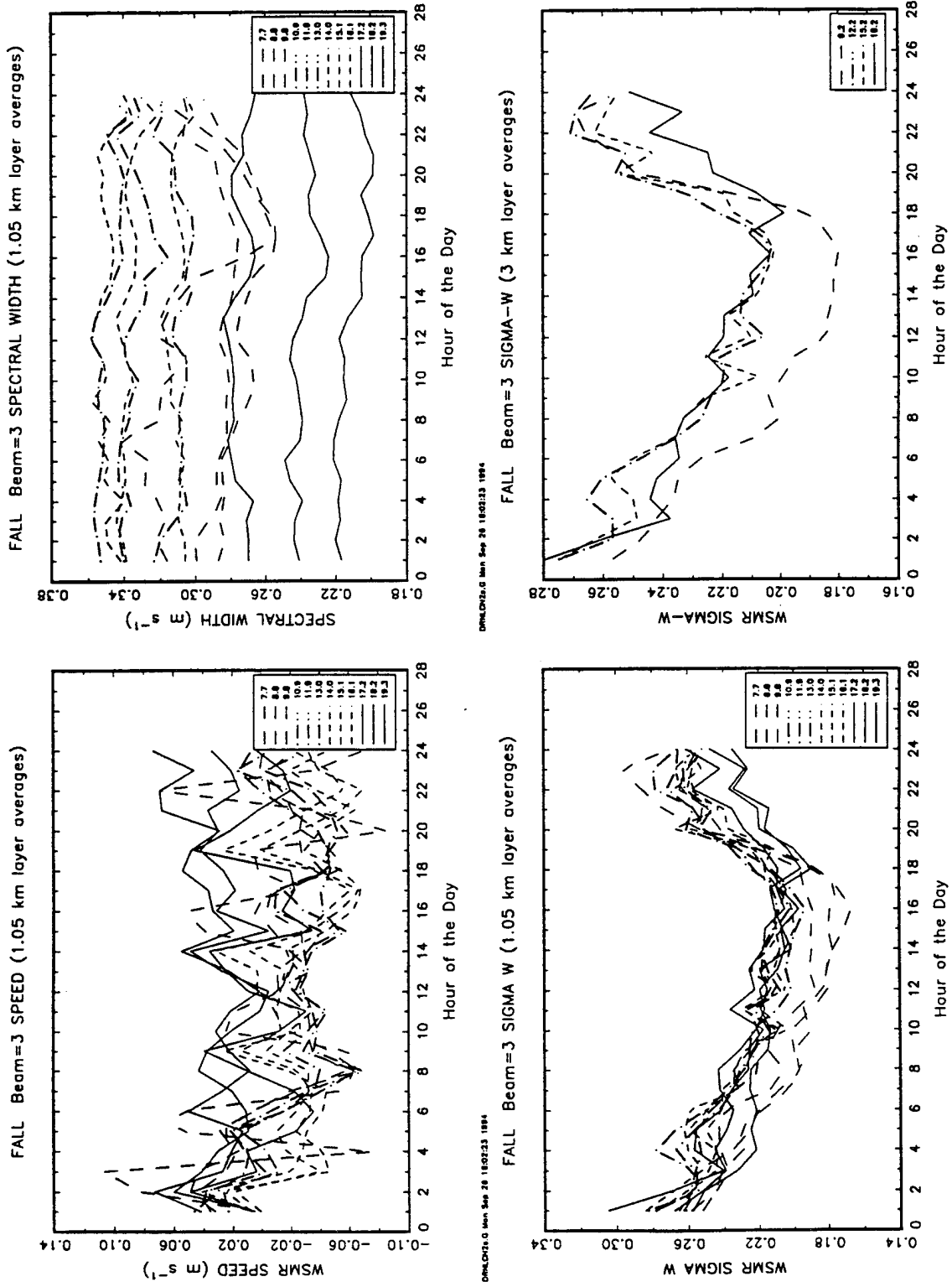


Figure 26. Diurnal variations of windspeed, spectral width, and σ_w during fall on the beam in the meridional plane.

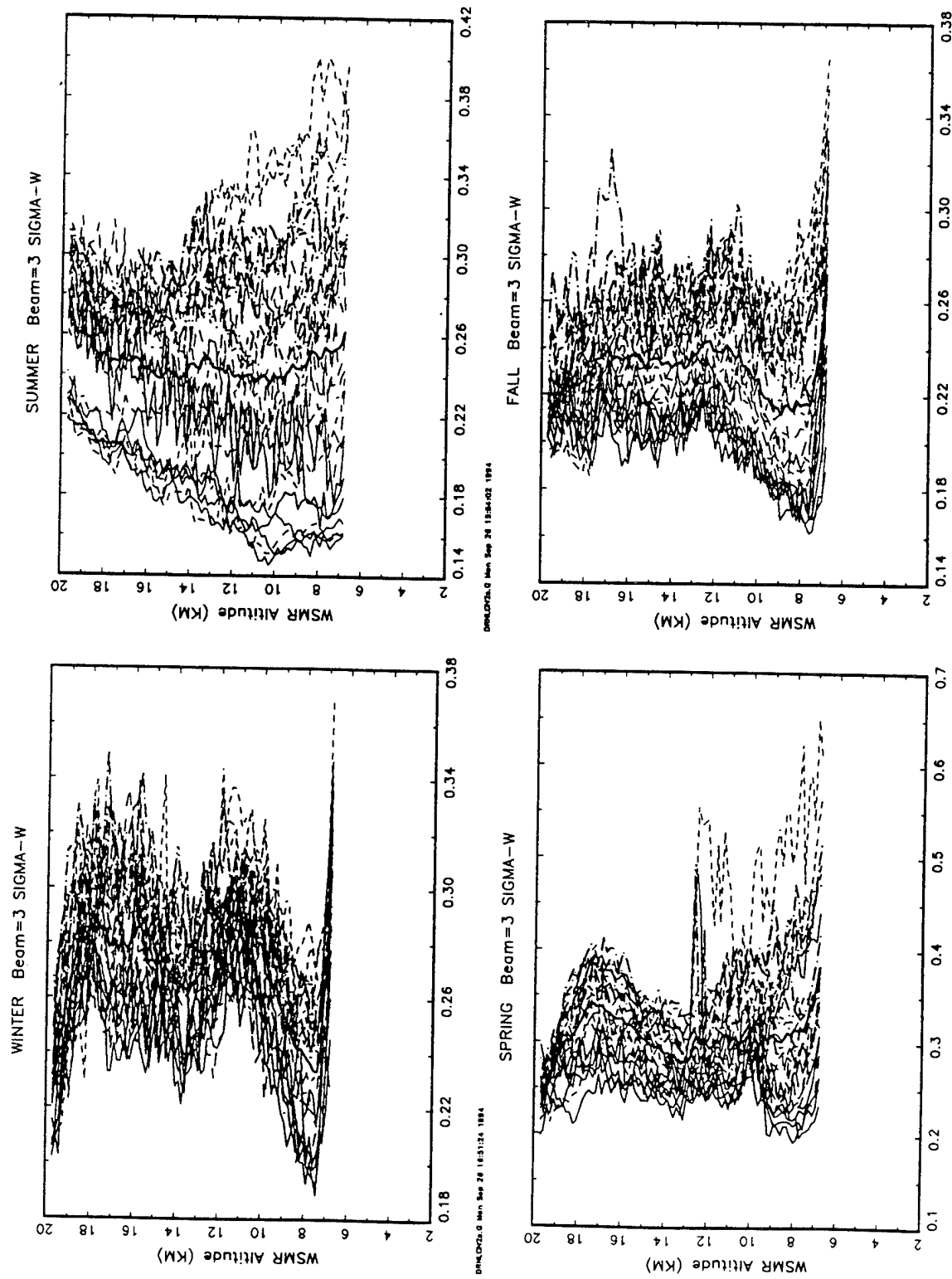


Figure 27. Vertical profiles of σ_w sorted by hour of the day for each season. Successive 6-h periods have different line types. The mean over 24 h is shown by a bold line.

6. Changes of Log C_N^2 with Background Weather Conditions

There have been several efforts to model C_N^2 as a function of other, more easily measured atmospheric variables. One of the first models was that of Hufnagel (1974), whose independent variable was mean windspeed aloft. More sophisticated models, such as those of Warnock and VanZandt (1985) and Dewan et al. (1993), require a computer to produce a profile of C_N^2 and detailed knowledge of the vertical profile of temperature, humidity, and winds. The goal of this section is to develop simple regression models that could be used to construct an estimated profile of C_N^2 with relatively simple and commonly available input data and a hand calculator.

Time-series plots of C_N^2 were compared with other variables available from the radar (for example, horizontal windspeed and direction, and standard deviation of the vertical velocity) and with daily weather maps at the surface and aloft. Also, numerical correlation analyses were made between C_N^2 and other radar variables. During the fall through the spring, the tropospheric C_N^2 responds strongly with the airmass changes marked by the passage of fronts. Gossard (1977) discusses the relationship of tropospheric C_N^2 to airmass type. A good indicator of airmass changes is the meridional windspeed in the midtroposphere, near 500 hPa. During the winter season, C_N^2 at 5.6 km correlated more closely with v at 5.6 km than with any other radar variable, including spectral width. This relation can be understood as the winds are from the south ahead of an eastward moving trough at 500 hPa and from the north while behind it.

The close correlation of $\log C_N^2$ and v is illustrated in figure 28 using data from January 1991. The upper left panel of figure 28 shows time-series plots of meridional windspeed normalized by its standard deviation over the 233 data points used and of $\log C_N^2$ similarly normalized. The correlation is 0.407 and can easily be detected by inspection. The upper right panel shows a scatter plot of $\log C_N^2$ as a function of v , along with the linear regression line for this data set. The regression coefficients for all data during winter are given in table 1. The lower left panel gives a scatter plot of $\log C_N^2-U$ versus $\log C_N^2-V$ for January 1991. That the two variables are not perfectly correlated may result from different sampling volumes, a true anisotropy in atmospheric turbulence,

calibration errors in one or both radar beam systems, or other factors that are beyond the scope of this study. The lower right panel of figure 28 is similar to the upper right panel, except for $\log C_N^2 \cdot V$ as a function of meridional wind.

It was noted earlier that C_N^2 is relatively constant through the lower stratosphere; thus, in an effort to keep this model as simple as possible, the stratospheric values are represented by the median value from 12 to 18 km. The median $\log C_N^2$ correlated most closely with the standard deviation of vertical velocity σ_w in the stratosphere at 12 to 18 km. (Median values of C_N^2 are summarized in figure 30 for convenient reference.) The physical basis for this correlation is likely that increased σ_w implies increased gravity wave amplitudes, which in turn imply more wave breaking and more small-scale turbulence. A proxy indicator was sought because σ_w is not a commonly reported variable. The median C_N^2 was found to correlate closely with zonal windspeed at 5.6 km (near 500 hPa), probably because the mountain ridges near WSMR run generally north-south, so the zonal wind is perpendicular to the ridges and thus launches vertically propagating gravity waves which break in the stratosphere, creating turbulence and enhancing C_N^2 . Nastrom and Eaton (1993a) also found strong coupling of $\log C_N^2$ with tropospheric zonal windspeed. Figure 29 shows a time-series plot of zonal windspeed at 5.6 km and the median $\log C_N^2$ at 12 to 18 km for a period in spring 1991 (left panel) and a scatter plot of these two variables (right panel). The equation for the regression line in the right panel is given at the bottom of the panel.

Regression coefficients for all seasons are included in the table along with the correlation coefficient of $\log C_N^2$ with the independent variable. During winter, the correlation of $\log C_N^2$ (12 to 18 km) with zonal windspeed is not high. If information on σ_w is available, it should be used instead of u , since it has a much higher correlation (0.38). The proper regression equation in this case is $\log C_N^2 = -18.06 + 0.51 * \sigma_w$ (12 km). The value of C_N^2 at 5.6 km does not correlate well with any available meteorological variable during the summer. Clearly, C_N^2 in the troposphere is most closely related to the level of humidity, and it is likely that during summer humidity is generally a local variable not controlled by the large-scale flow.

The regression model implied by figures 28 and 29 and the above discussion can be used as follows:

- Use the current or forecast 500 hPa meridional windspeed to estimate $\log C_N^2$ at 5.6 km.
- Use the current or forecast 500 hPa zonal windspeed to estimate $\log C_N^2$ at 12 to 18 km.
- Plot the estimates on a graph and draw a line from the value at 12 km through that at 5.6 km.
- Extrapolate the estimates below 5.6 km to the top of the planetary boundary layer (PBL). This model is for the free troposphere and thus not appropriate for the PBL.

Keep in mind that this model was developed using data from WSMR and is likely appropriate only for similar terrain and climatic conditions. Warnock et al. (1988) and Otten and Rose (1985) noted differences in C_N^2 as a function of underlying terrain.

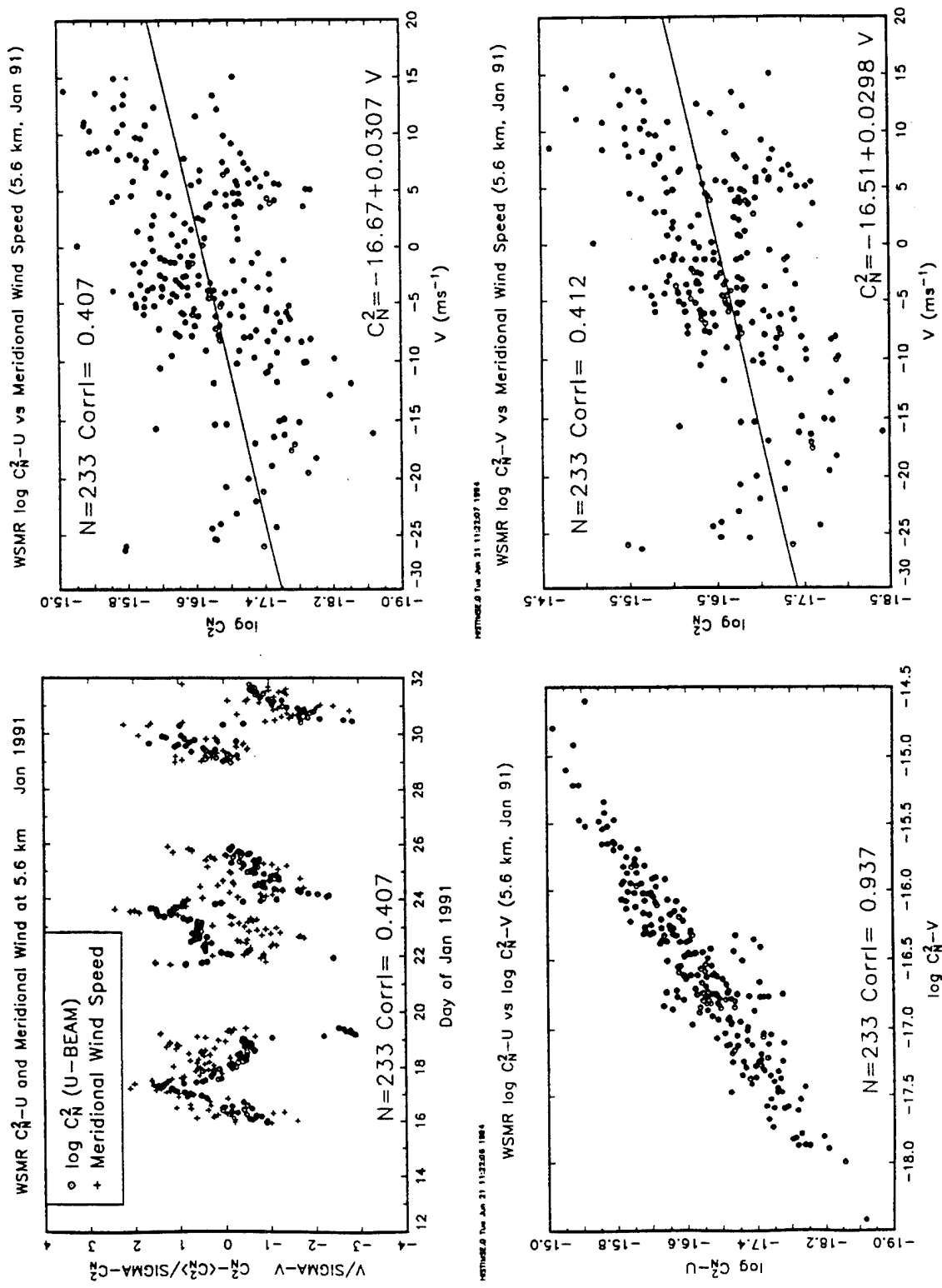


Figure 28. Correlation and regression relations of $\log C_N^2$ and v at 5.6 km.

Table 1. Regression coefficients for $\log C_N^2$ as a function of u and v at WSMR (see text)

	Dec-Jan-Feb	Mar-Apr-May	Jun-Jul-Aug	Sept-Oct-Nov
Number	2,484	2,046	2,104	3,242
Regression	C_N^2 (5.6 km) = $a+b*v(5.6 \text{ km})$			
a	-16.47	-16.57	-15.21	-16.20
b	0.0336	0.0136	0.0040	0.034
correlation	0.42	0.16	0.03	0.27
Regression	C_N^2 (12-18 km) = $a+b*u(5.6 \text{ km})$			
a	-17.90	-18.06	-17.92	-18.06
b	-0.00137	0.012	0.0050	0.0085
correlation	-0.06	0.42	0.12	0.30

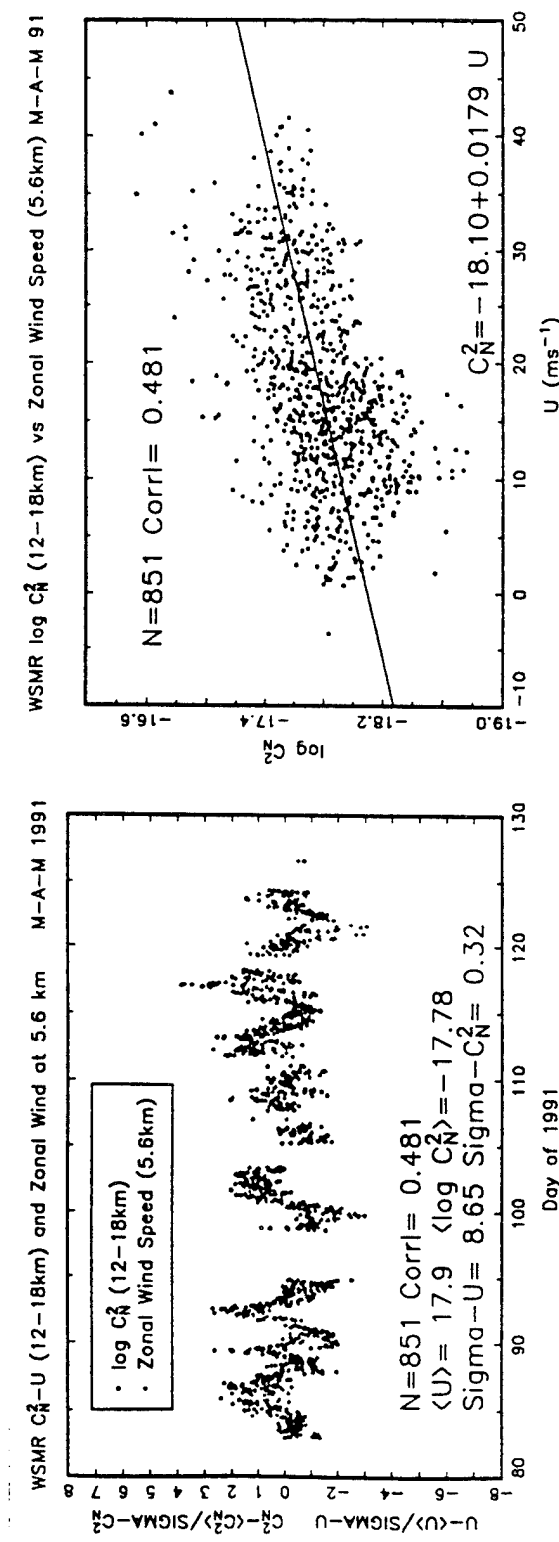


Figure 29. Correlation and regression relations of $\log C_N^2$ (the median value from 12 to 18 km) with u at 5.6 km.

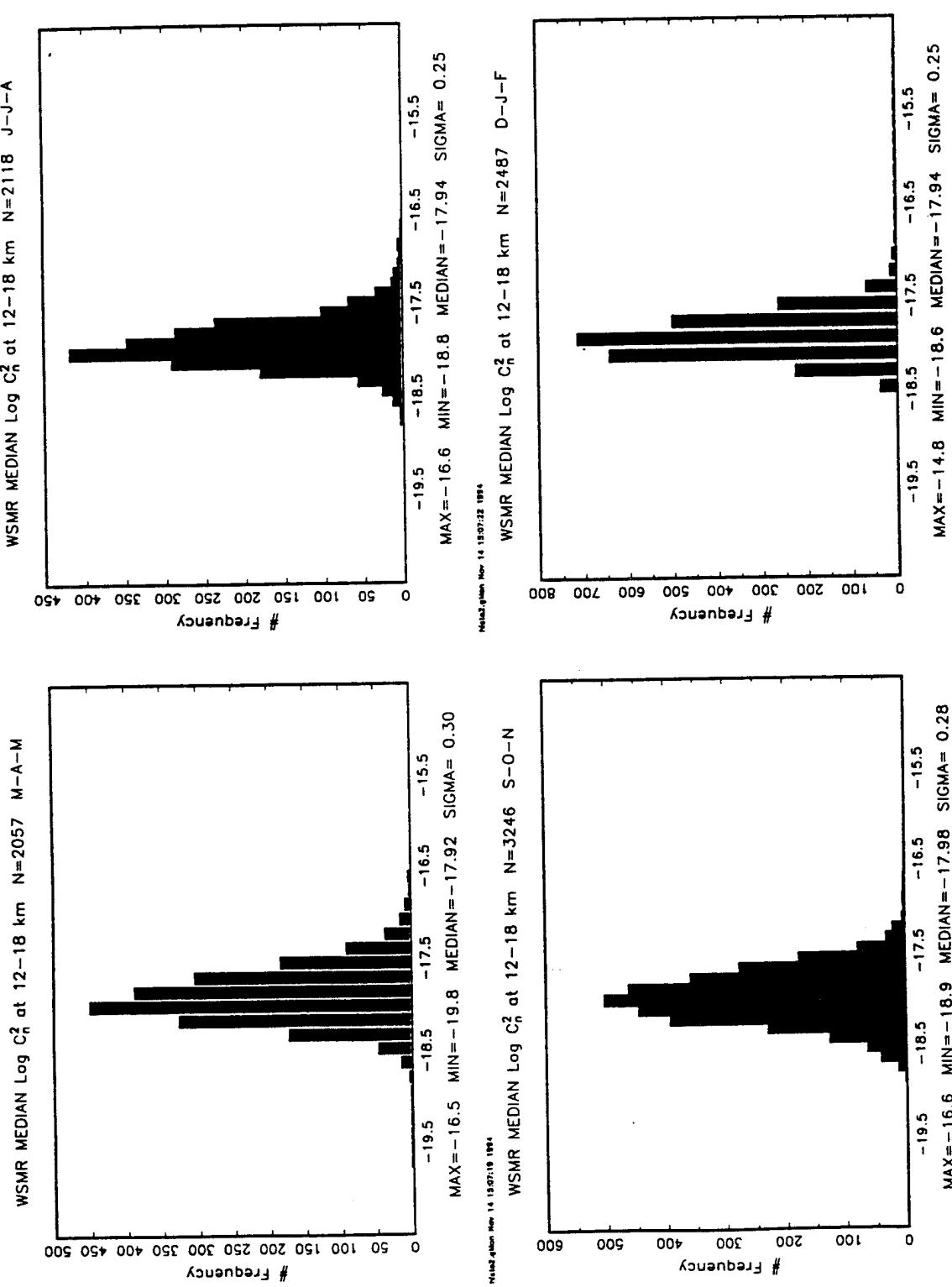


Figure 30. Frequency distribution of $\log C_n^2$ at 12 to 18 km for all seasons. Also, the temporal standard deviation (sigma) is included on each panel.

7. Summary and Conclusions

A relatively very large data set was collected with the 50-MHz profiler at WSMR. The available data span the period January 1991 through April 1994 and cover the height range from approximately 5 to 20 km, with a 150-m vertical resolution and a 3-min time resolution. The data set is suitable for climatological studies of atmospheric variables such as windspeed and direction, vertical wind variability, and indicators of small-scale turbulence such as spectral width and C_N^2 . This report has emphasized the seasonal, interannual, diurnal, and weather-related changes in C_N^2 and wind.

Above the tropopause, there are only small changes with season of C_N^2 . Also, above the troposphere, there are only small diurnal changes of C_N^2 , usually less than a few decibels.

The autocorrelation function of C_N^2 can be modeled as the sum of a random process and a first-order autoregressive process, with a very small contribution from a first-order moving-average process. The shape of the autocorrelation function suggests that the average time between statistically independent observations of C_N^2 ranges from about 2 to 4 h in both the troposphere and stratosphere. During periods of active weather systems, the average time is much less.

Diurnal variations of $\log C_N^2$ are relatively small. Spectral width shows a maximum in the troposphere during local afternoon, as does the standard deviation of vertical velocity. Mean windspeeds show a large diurnal variation in the stratosphere during summer.

The vertical profile of C_N^2 is related to temperature and humidity gradients and small-scale turbulence intensity. As a result of these relations, C_N^2 in the troposphere is correlated with airmass changes indicated by the tropospheric meridional windspeed, whereas C_N^2 in the stratosphere is correlated with gravity wave activity indicated by the tropospheric zonal windspeed. These correlations were used in developing a simple regression model that would be suitable for

estimating the vertical profile of C_N^2 with only simple, commonly available input variables and a hand calculator.

This model might be improved by sorting the data according to another independent variable(s) such as temperature or static stability. No rawinsonde data were used in this study. Also, the data could be sorted by distance from the tropopause rather than by geometric altitude; the tropopause is a dynamic variable that can be estimated from the backscattered radar power (Gage 1990).

References

Chadwick, R. B., and K. P. Moran, "Long-Term Measurements of C_N^2 in the Boundary Layer," *Radio Sci.*, **15**, p 355-361, 1980.

Dewan, E. M., R. E. Good, R. Beland, and J. Brown, *A Model for C_N^2 (Optical Turbulence) Profiles Using Radiosonde Data*, PL-TR-93-2043, Envir. Res. Papers No. 1121, Phillips Laboratory, p 41, 1993.

Frisch, A. S., B. L. Weber, D. B. Wuertz, R. G. Strauch, and D. A. Merritt, "The Variations of C_N^2 Between 4 and 18 km Above Sea Level as Measured Over 5 Years," *J. Appl. Meteor.*, **29**, p 645-651, 1990.

Gage, K. S., "Radar Observations of the Free Atmosphere: Structure and Dynamics, In Radar in Meteorology," ed. David Atlas, American Meteorological Society, Boston, p 534-565, 1990.

Gossard, E. E., "Refractive Index Variance and its Height Distribution in Different Air Masses," *Radio Sci.*, **12**, p 89-105, 1977.

Hocking, W. K., "Measurement of Turbulent Energy Dissipation Rates in the Middle Atmosphere by Radar Techniques: A Review," *Radio Sci.*, **20**, p 1403-1422, 1985.

Hufnagel, R. E., "Variations of Atmospheric Turbulence," *Digest of Technical Papers, Topical Meeting on Optical Propagation Through Turbulence, Wa 1-1 to Wa 1-4*, Optical Society of America, Washington, D.C., 1974.

Nastrom, G. D., K. S. Gage, and W. L. Ecklund, "Variability of Turbulence, 4-20 km, in Colorado and Alaska from MST Radar Observations," *J. Geophys. Res.*, **91**, p 6722-6734, 1986.

Nastrom, G. D., and F. D. Eaton, "The Coupling of Gravity Waves and Turbulence at White Sands, New Mexico, from VHF Radar Observations," *J. Appl. Meteor.*, **32**, p 81-87, 1993a.

Nastrom, G. D., and F. D. Eaton, "The Onset of the Summer Monsoon over White Sands Missile Range, New Mexico, as Seen by VHF Radar," *J. Geophys. Res.*, **98**, p 23235-23243, 1993b.

Nastrom, G. D., and T. E. VanZandt, "Mean Vertical Motions Seen by Radar Wind Profilers," *J. Appl. Meteor.*, **33**, p 984-995, 1994.

Otten, L. J., and W. C. Rose, *Airborne Observations of Tropopause Turbulence*, AIAA-85-0342, Amer. Instit. Aeron. Astron., p 5, 1985.

Sato, K., "Vertical Wind Disturbances in the Troposphere and Lower Stratosphere Observed by the MU Radar," *J. Atmos. Sci.*, **47**, p 2803-2817, 1990.

Sato, K., "Vertical Wind Disturbances in the Afternoon of Mid-Summer Revealed by the MU Radar," *Geophys. Res. Lett.*, **19**, p 1943-1946, 1992.

Tsuda, T., P. T. May, T. Sato, S. Kato, and S. Fukao, "Simultaneous Observations of Reflection Echoes and Refractive Index Gradient in the Troposphere and Lower Stratosphere," *Radio Sci.*, **23**, p 655-665, 1988.

Warnock, J. M., R. R. Beland, J. H. Brown, W. L. Clark, F. D. Eaton, L. D. Favier, K. S. Gage, J. L. Green, W. H. Hatch, J. R. Hines, E. A. Murphy, G. D. Nastrom, W. A. Peterson, and T. E. VanZandt, "Comparison Among Clear-Air Radar, Thermosonde and Optical Measurements and Model Estimates of C_N^2 Made in very Flat Terrain Over Illinois," Presented at the Fourth Workshop on MST Radars, Kyoto, Nov 29-Dec 2, *Handbook for MAP*, **28**, p 432-438, 1988.

Warnock, J. M., and T. E. VanZandt, NOAA TM-ERL-AL-10, *A Statistical Model to Estimate the Refractivity Turbulence Structure Constant C_N^2 in the Free Atmosphere*, **175**, 1985.

Appendix A

WSMR Data Inventory

WSMR Data Inventory 1991–1994

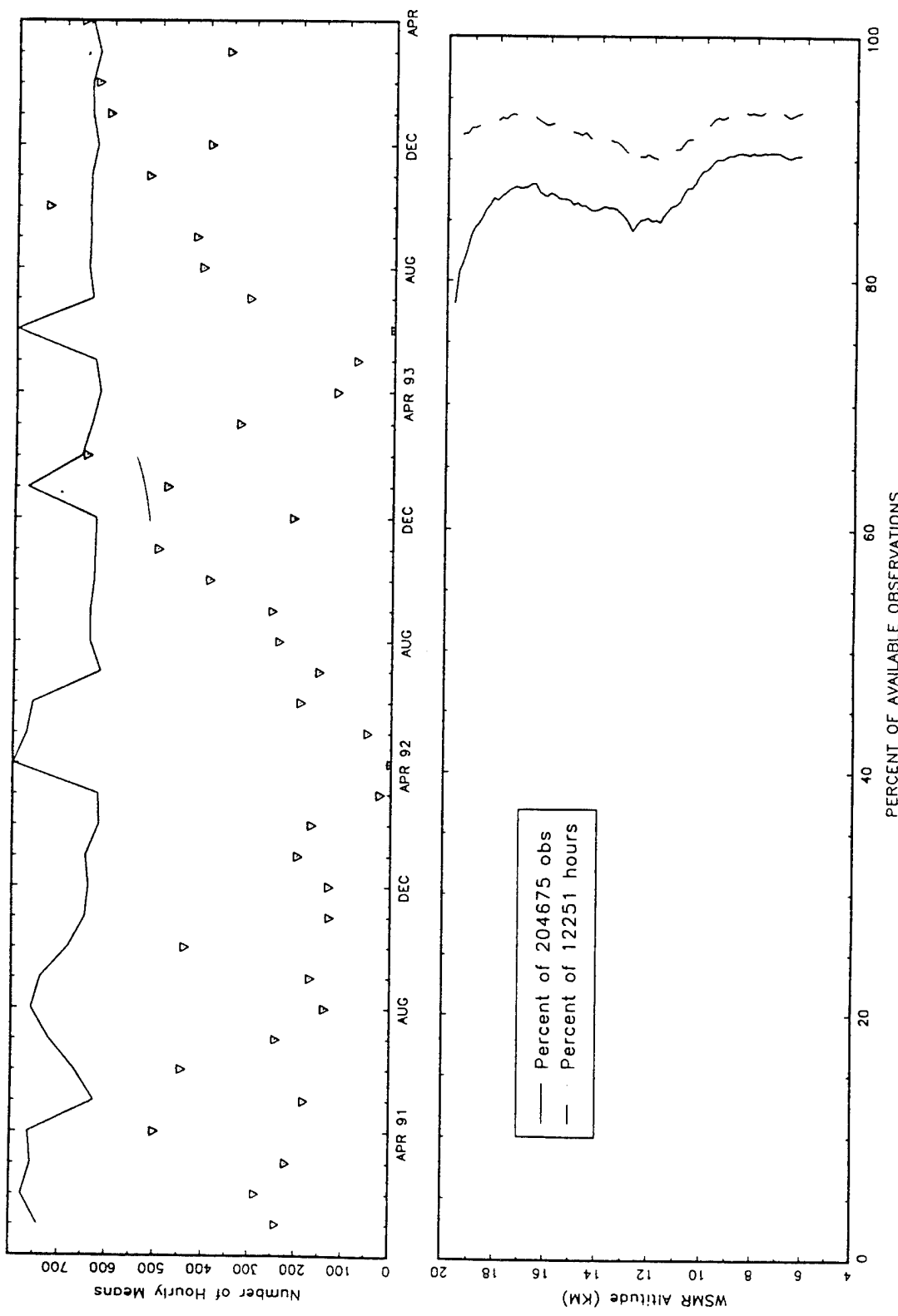


Figure A-1. Monthly inventory of the data available at WSMR during January 1991 through April 1994. (Top) Symbols show the number of hourly means during each month; the solid line shows the average number of observations during each hour, with 20 observations corresponding to full scale. (Bottom) The percent of observations or hourly means (only hours with five or more profiles were analyzed) available as a function of altitude.

Appendix B

Examples of Monthly Charts

Examples of the charts prepared for each month, January 1991 to April 1994. These charts were used to check data continuity, for comparison with standard weather maps, and as an analyses tool. The time-series plots are of hourly mean values.

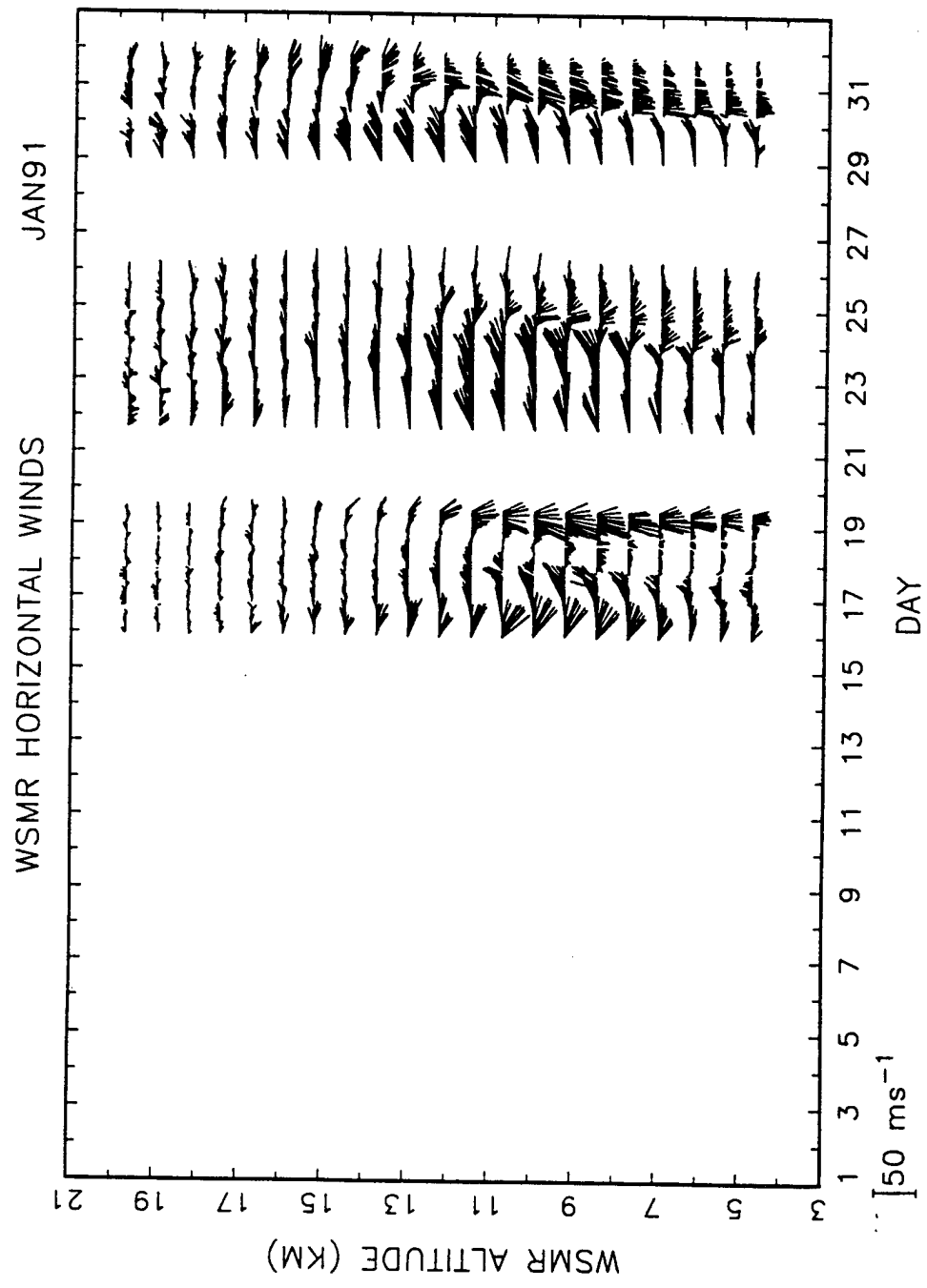


Figure B-1. Horizontal windspeeds plotted as vectors (estimated from the oblique radial velocities assuming the vertical velocity is zero).

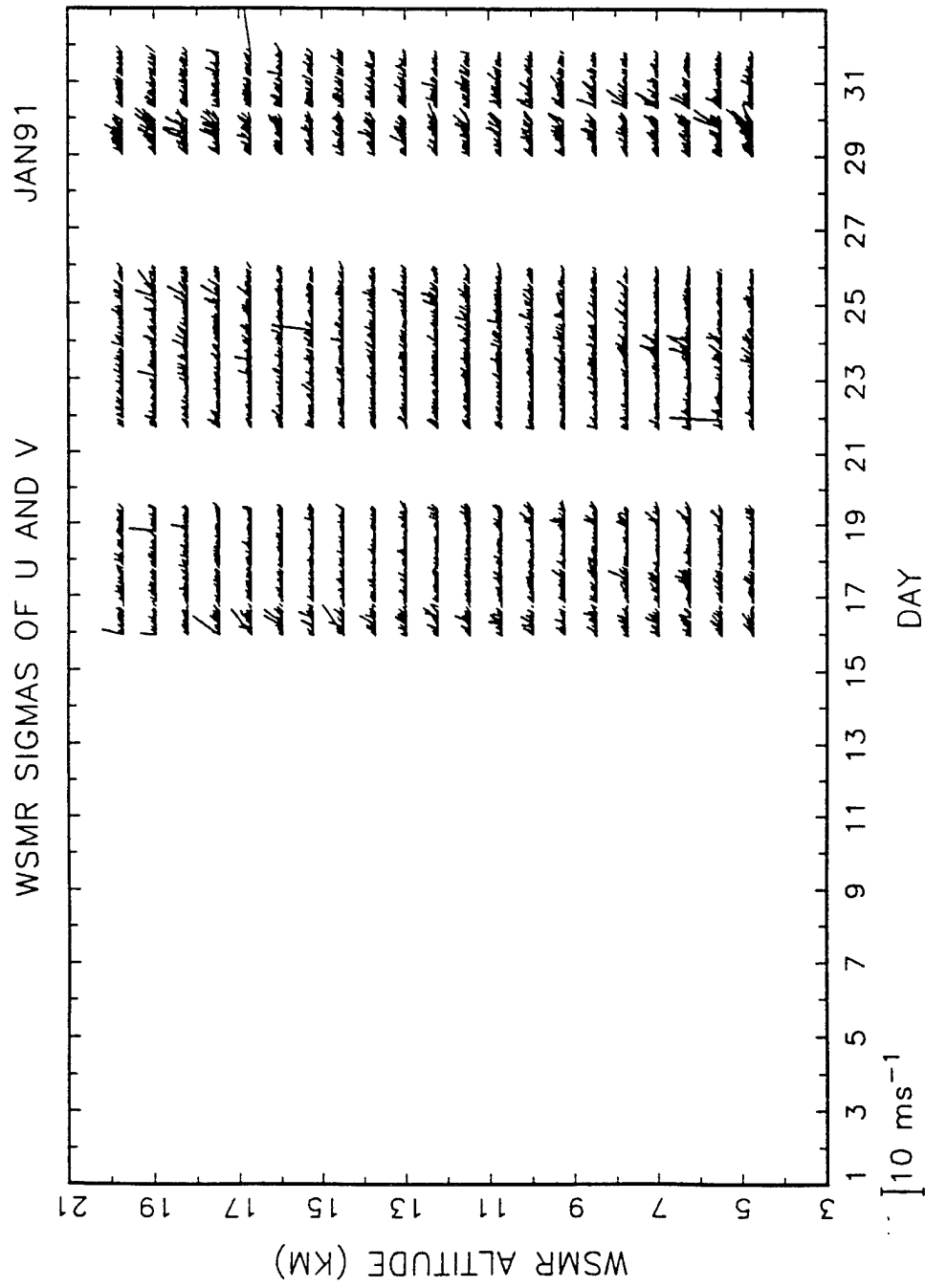


Figure B-2. Standard deviation of u and v associated with the means in the chart shown in figure B-1, plotted as vectors.

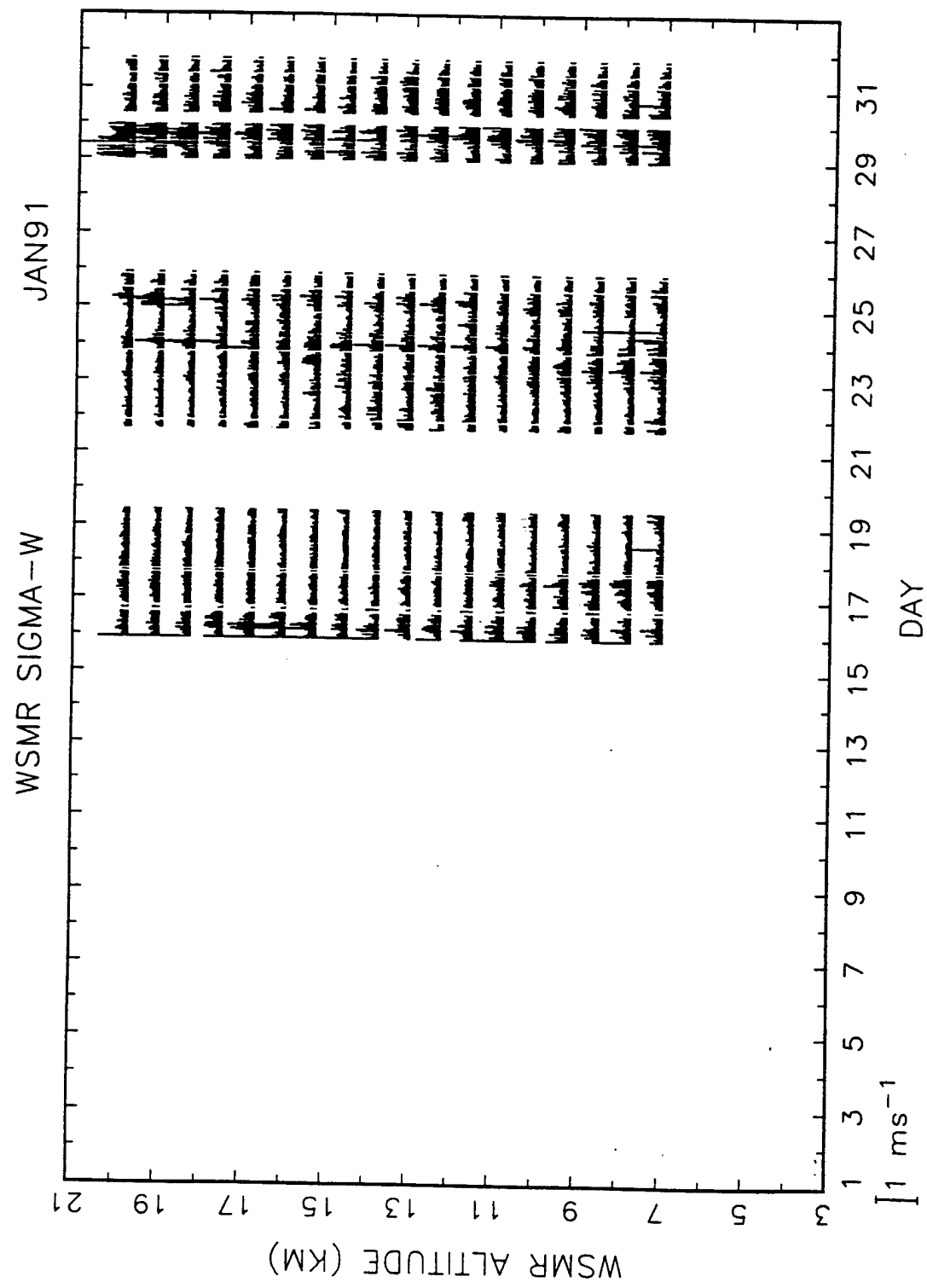


Figure B-3. Hourly standard deviation of vertical velocity.

JAN 91

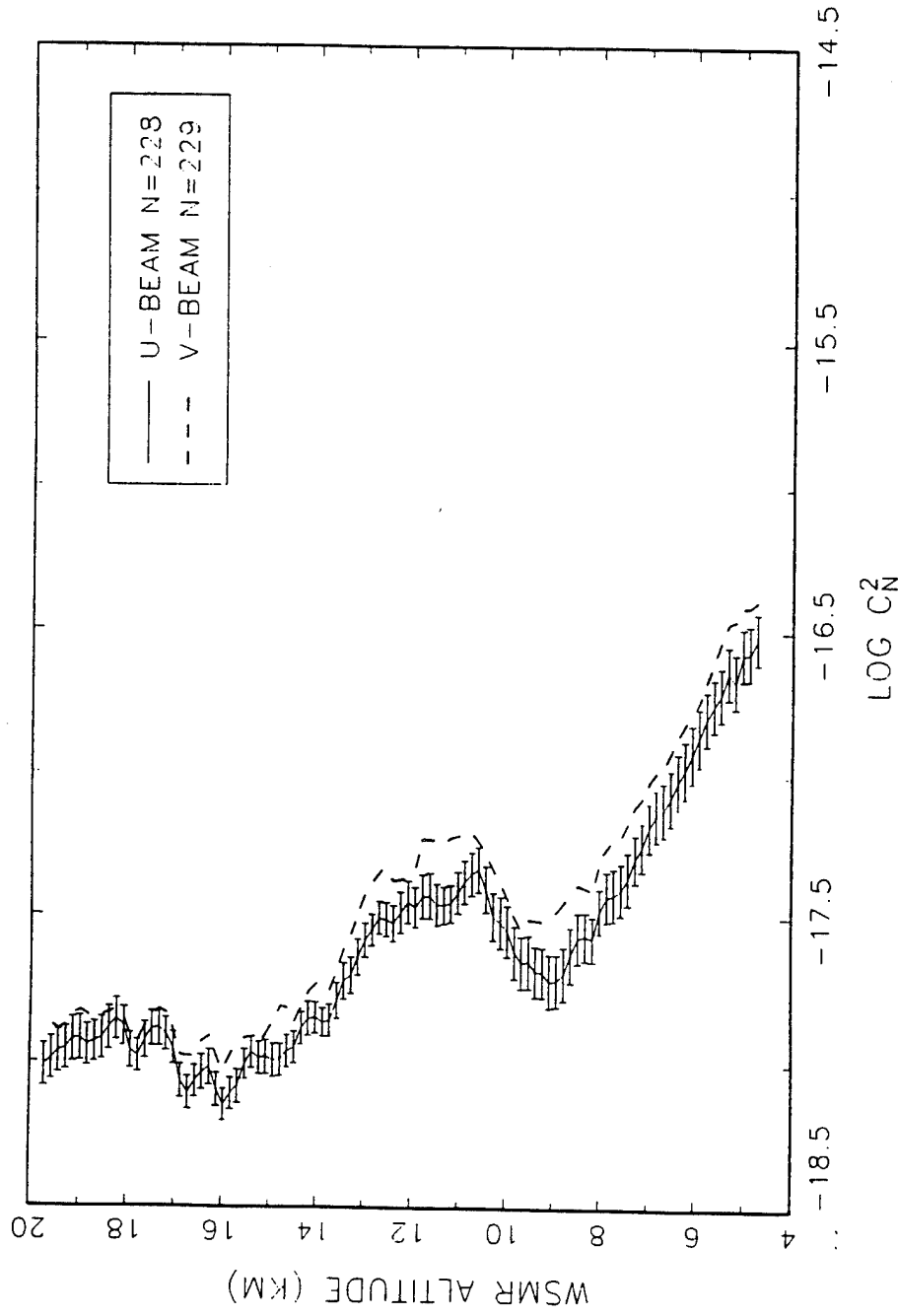
WSMR MONTHLY MEAN C_N^2 

Figure B-4. Vertical profiles of the monthly means of $\log C_N^2$ for the oblique beams. The error bars extend one standard error of the mean from the mean.

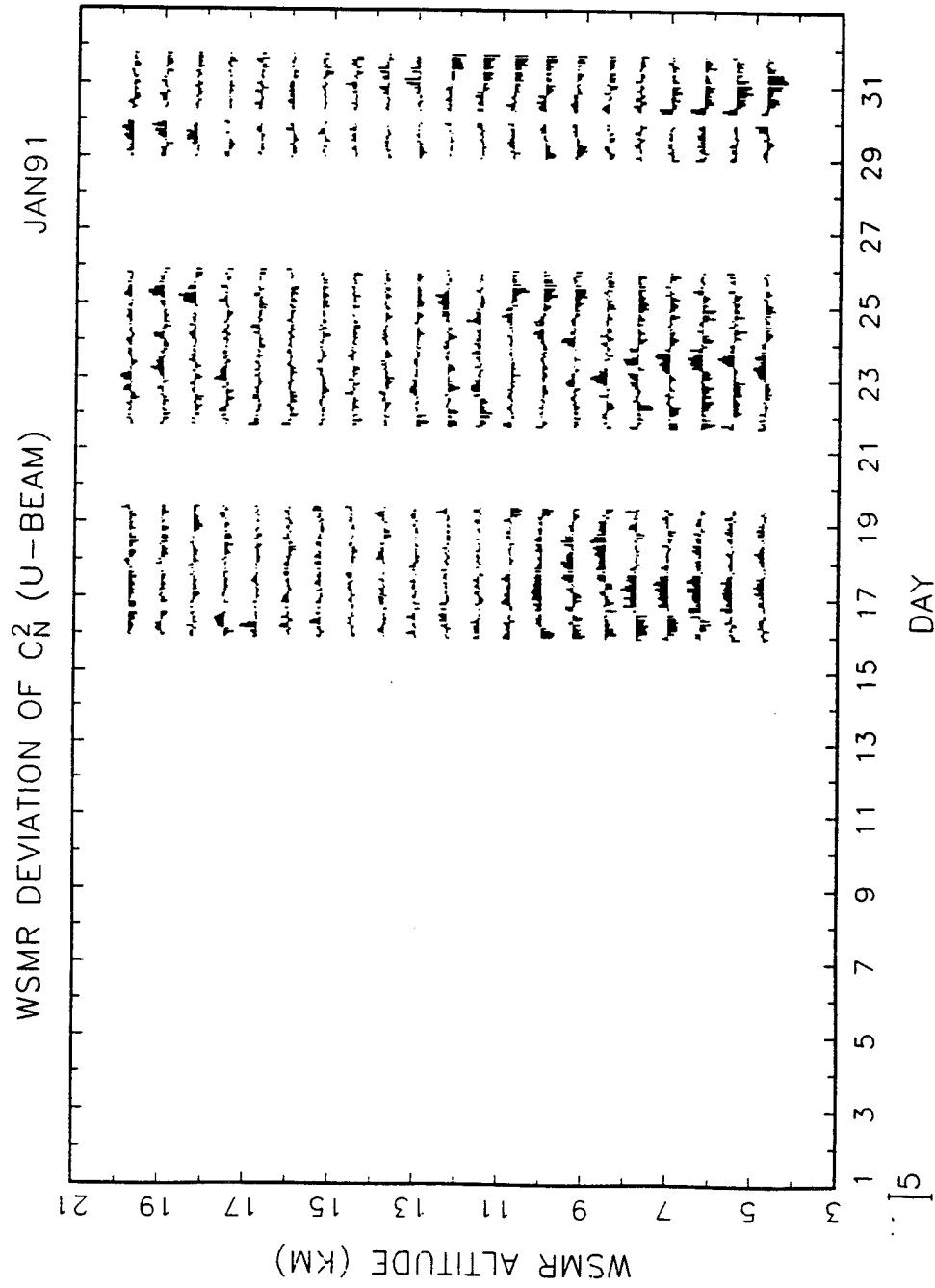


Figure B-5. Deviations of hourly mean $\log C_N^2$ from the monthly means in the chart shown in figure B-4.

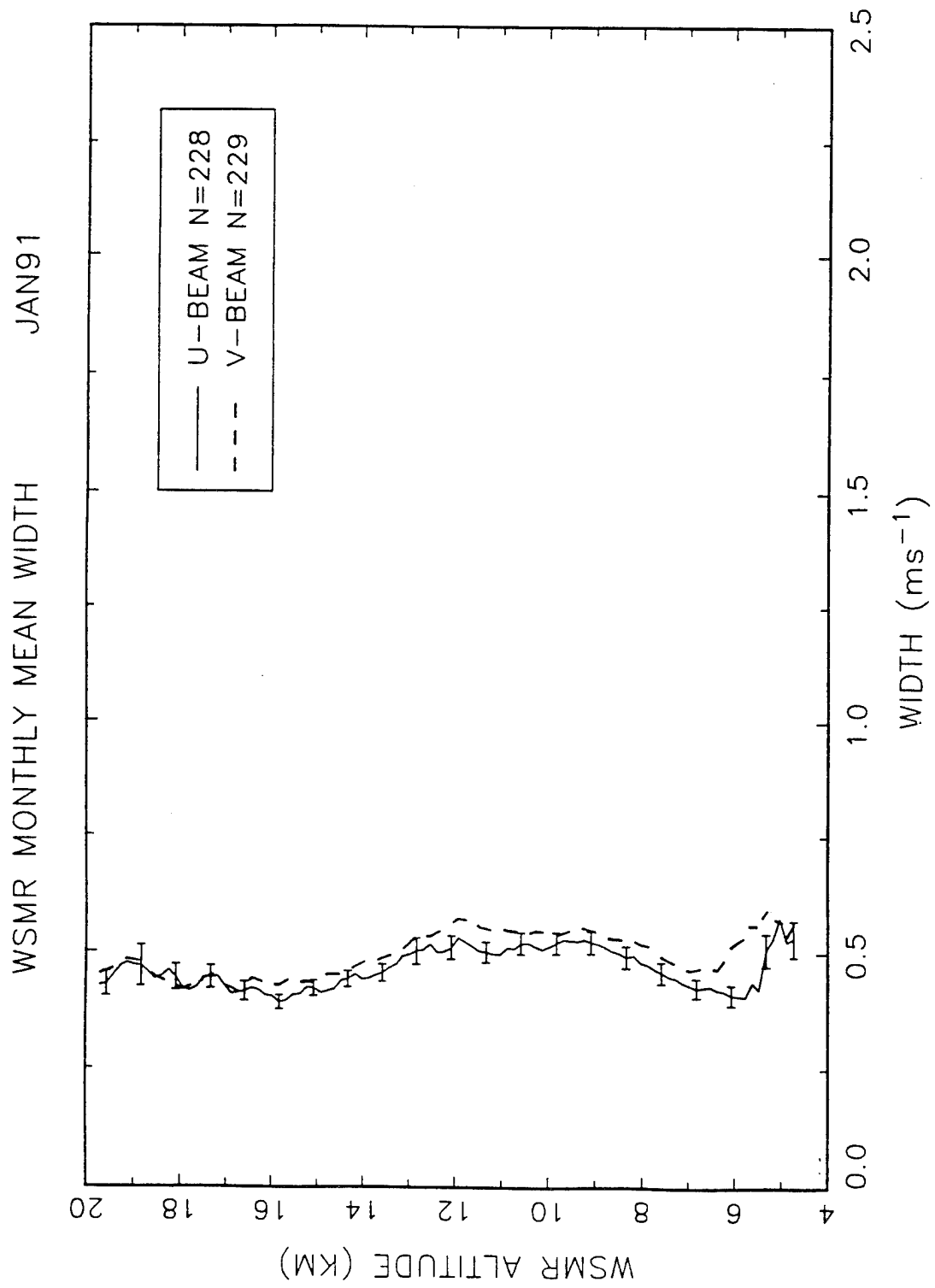


Figure B-6. Vertical profiles of the monthly means for spectral width.

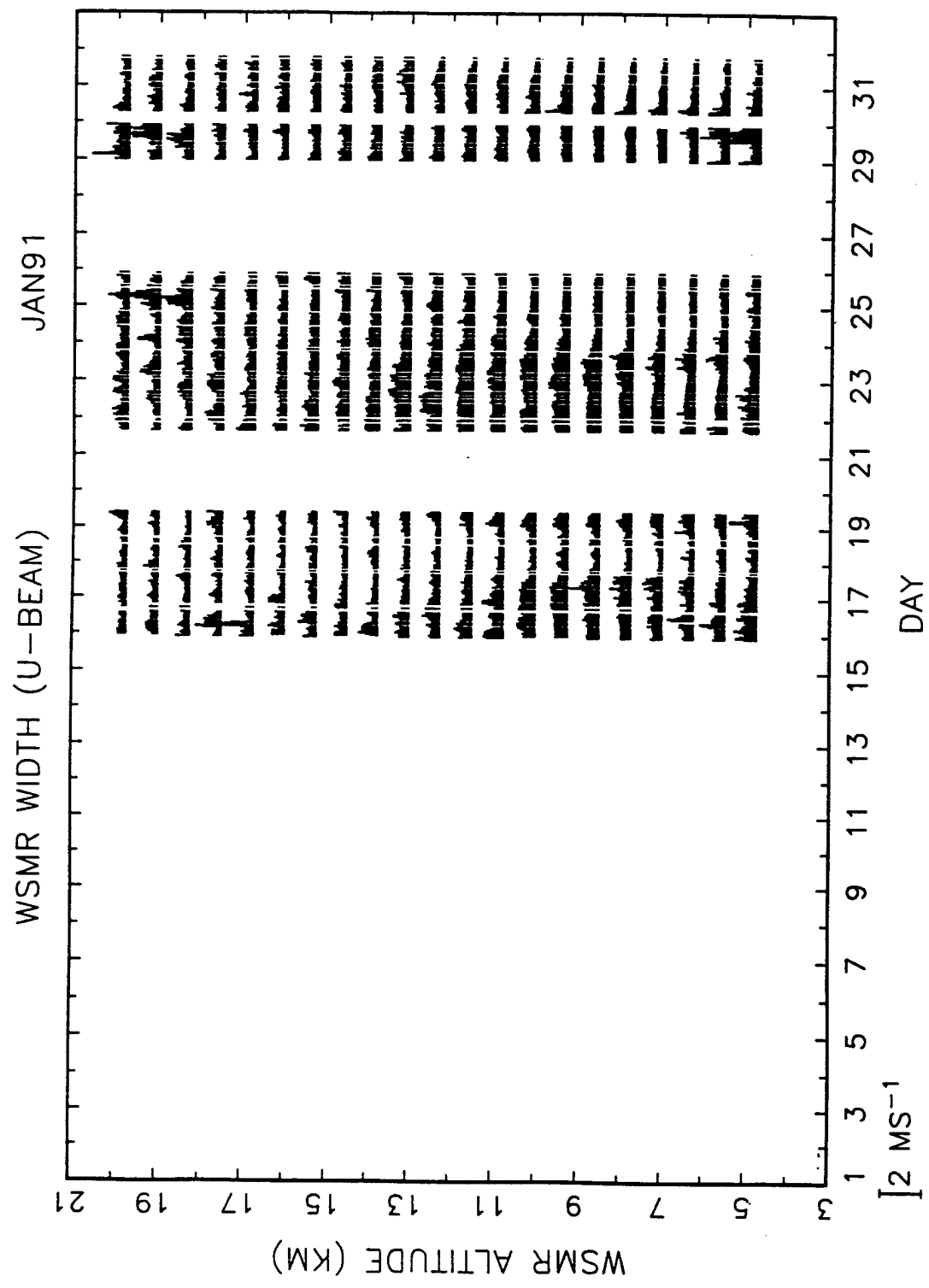


Figure B-7. Deviations of spectral width from the monthly means in the chart shown in figure B-6.

Distribution

	Copies
ARMY CHEMICAL SCHOOL ATZN CM CC ATTN MR BARNES FT MCCLELLAN AL 36205-5020	1
NASA MARSHAL SPACE FLT CTR ATMOSPHERIC SCIENCES DIV E501 ATTN DR FICHTL HUNTSVILLE AL 35802	1
NASA SPACE FLT CTR ATMOSPHERIC SCIENCES DIV CODE ED 41 1 HUNTSVILLE AL 35812	1
ARMY STRAT DEFNS CMND CSSD SL L ATTN DR LILLY PO BOX 1500 HUNTSVILLE AL 35807-3801	1
ARMY MISSILE CMND AMSMI RD AC AD ATTN DR PETERSON REDSTONE ARSENAL AL 35898-5242	1
ARMY MISSILE CMND AMSMI RD AS SS ATTN MR H F ANDERSON REDSTONE ARSENAL AL 35898-5253	1
ARMY MISSILE CMND AMSMI RD AS SS ATTN MR B WILLIAMS REDSTONE ARSENAL AL 35898-5253	1

ARMY MISSILE CMND AMSMI RD DE SE ATTN MR GORDON LILL JR REDSTONE ARSENAL AL 35898-5245	1
ARMY MISSILE CMND REDSTONE SCI INFO CTR AMSMI RD CS R DOC REDSTONE ARSENAL AL 35898-5241	1
ARMY MISSILE CMND AMSMI REDSTONE ARSENAL AL 35898-5253	1
ARMY INTEL CTR AND FT HUACHUCA ATSI CDC C FT HUACHUCA AZ 85613-7000	1
CMD 420000D C0245 ATTN DR A SHLANTA NAVAIRWARCENWPNDIV 1 ADMIN CIR CHINA LAKE CA 93555-6001	1
PACIFIC MISSILE TEST CTR GEOPHYSICS DIV ATTN CODE 3250 POINT MUGU CA 93042-5000	1
LOCKHEED MIS & SPACE CO ATTN KENNETH R HARDY ORG 91 01 B 255 3251 HANOVER STREET PALO ALTO CA 94304-1191	1
NAVAL OCEAN SYST CTR CODE 54 ATTN DR RICHTER SAN DIEGO CA 92152-5000	1

METEOROLOGIST IN CHARGE KWAJALEIN MISSILE RANGE PO BOX 67 APO SAN FRANCISCO CA 96555	1
DEPT OF COMMERCE CTR MOUNTAIN ADMINISTRATION SPPRT CTR LIBRARY R 51 325 S BROADWAY BOULDER CO 80303	1
DR HANS J LIEBE NTIA ITS S 3 325 S BROADWAY BOULDER CO 80303	1
NCAR LIBRARY SERIALS NATL CTR FOR ATMOS RSCH PO BOX 3000 BOULDER CO 80307-3000	1
DEPT OF COMMERCE CTR 325 S BROADWAY BOULDER CO 80303	1
DAMI POI WASH DC 20310-1067	1
MIL ASST FOR ENV SCI OFC OF THE UNDERSEC OF DEFNS FOR RSCH & ENGR R&AT E LS PENTAGON ROOM 3D129 WASH DC 20301-3080	1
DEAN RMD ATTN DR GOMEZ WASH DC 20314	1
ARMY INFANTRY ATSH CD CS OR ATTN DR E DUTOIT FT BENNING GA 30905-5090	1
AIR WEATHER SERVICE TECH LIBRARY FL4414 3 SCOTT AFB IL 62225-5458	1

USAFETAC DNE ATTN MR GLAUBER SCOTT AFB IL 62225-5008	1
HQ AWS DOO 1 SCOTT AFB IL 62225-5008	1
PHILLIPS LABORATORY PL LYP ATTN MR CHISHOLM HANSCOM AFB MA 01731-5000	1
ATMOSPHERIC SCI DIV GEOPHYSICS DIRCTRT PHILLIPS LABORATORY HANSCOM AFB MA 01731-5000	1
PHILLIPS LABORATORY PL LYP 3 HANSCOM AFB MA 01731-5000	1
RAYTHEON COMPANY ATTN DR SONNENSCHEIN 528 BOSTON POST ROAD SUDBURY MA 01776 MAIL STOP 1K9	1
ARMY MATERIEL SYST ANALYSIS ACTIVITY AMXSY ATTN MP H COHEN APG MD 21005-5071	1
ARMY MATERIEL SYST ANALYSIS ACTIVITY AMXSY AT ATTN MR CAMPBELL APG MD 21005-5071	1
ARMY MATERIEL SYST ANALYSIS ACTIVITY AMXSY CR ATTN MR MARCHET APG MD 21005-5071	1

ARL CHEMICAL BIOLOGY NUC EFFECTS DIV AMSRL SL CO APG MD 21010-5423	1
ARMY MATERIEL SYST ANALYSIS ACTIVITY AMXSY APG MD 21005-5071	1
ARMY MATERIEL SYST ANALYSIS ACTIVITY AMXSY CS ATTN MR BRADLEY APG MD 21005-5071	1
ARMY RESEARCH LABORATORY AMSRL D 2800 POWDER MILL ROAD ADELPHI MD 20783-1145	1
ARMY RESEARCH LABORATORY AMSRL OP SD TP TECHNICAL PUBLISHING 2800 POWDER MILL ROAD ADELPHI MD 20783-1145	1
ARMY RESEARCH LABORATORY AMSRL OP CI SD TL 2800 POWDER MILL ROAD ADELPHI MD 20783-1145	1
ARMY RESEARCH LABORATORY AMSRL SS SH ATTN DR SZTANKAY 2800 POWDER MILL ROAD ADELPHI MD 20783-1145	1
ARMY RESEARCH LABORATORY AMSRL 2800 POWDER MILL ROAD ADELPHI MD 20783-1145	1

NATIONAL SECURITY AGCY W21 ATTN DR LONGBOTHUM 9800 SAVAGE ROAD FT GEORGE G MEADE MD 20755-6000	1
OIC NAVSWC TECH LIBRARY CODE E 232 SILVER SPRINGS MD 20903-5000	1
ARMY RSRC OFC AMXRO GS ATTN DR BACH PO BOX 12211 RTP NC 27709	1
DR JERRY DAVIS NCSU PO BOX 8208 RALEIGH NC 27650-8208	1
US ARMY CECRL CECRL GP ATTN DR DETSCH HANOVER NH 03755-1290	1
ARMY ARDEC SMCAR IMI I BLDG 59 DOVER NJ 07806-5000	1
ARMY SATELLITE COMM AGCY DRCPM SC 3 FT MONMOUTH NJ 07703-5303	1
ARMY COMMUNICATIONS ELECTR CTR FOR EW RSTA AMSEL EW D FT MONMOUTH NJ 07703-5303	1
ARMY COMMUNICATIONS ELECTR CTR FOR EW RSTA AMSEL EW MD FT MONMOUTH NJ 07703-5303	1

ARMY DUGWAY PROVING GRD STEDP MT DA L 3 DUGWAY UT 84022-5000	1
ARMY DUGWAY PROVING GRD STEDP MT M ATTN MR BOWERS DUGWAY UT 84022-5000	1
DEPT OF THE AIR FORCE OL A 2D WEATHER SQUAD MAC HOLLOWAY AFB NM 88330-5000	1
PL WE KIRTLAND AFB NM 87118-6008	1
USAF ROME LAB TECH CORRIDOR W STE 262 RL SUL 26 ELECTR PKWY BLD 106 GRIFFISS AFB NY 13441-4514	1
AFMC DOW WRIGHT PATTERSON AFB OH 0334-5000	1
ARMY FIELD ARTLLRY SCHOOL ATSF TSM TA FT SILL OK 73503-5600	1
NAVAL AIR DEV CTR CODE 5012 ATTN AL SALIK WARMINISTER PA 18974	1
ARMY FOREGN SCI TECH CTR CM 220 7TH STREET NE CHARLOTTESVILLE VA 22901-5396	1
NAVAL SURFACE WEAPONS CTR CODE G63 DAHlgren VA 22448-5000	1

ARMY OEC CSTE EFS PARK CENTER IV 4501 FORD AVE ALEXANDRIA VA 22302-1458	1
ARMY CORPS OF ENGRS ENGR TOPOGRAPHICS LAB ETL GS LB FT BELVOIR VA 22060	1
TAC DOWP LANGLEY AFB VA 23665-5524	1
ARMY TOPO ENGR CTR CETEC ZC 1 FT BELVOIR VA 22060-5546	1
LOGISTICS CTR ATCL CE FT LEE VA 23801-6000	1
SCI AND TECHNOLOGY 101 RESEARCH DRIVE HAMPTON VA 23666-1340	1
ARMY NUCLEAR CML AGCY MONA ZB BLDG 2073 SPRINGFIELD VA 22150-3198	1
USATRA DOC ATCD FA FT MONROE VA 23651-5170	1
ARMY TRADOC ANALYSIS CTR ATRC WSS R WSMR NM 88002-5502	1
ARMY RESEARCH LABORATORY AMSRL BE S BATTLEFIELD ENVIR DIR WSMR NM 88002-5501	1

ARMY RESEARCH LABORATORY AMSRL BE E BATTLEFIELD ENVIR DIR WSMR NM 88002-5501	1
ARMY RESEARCH LABORATORY AMSRL BE W BATTLEFIELD ENVIR DIR WSMR NM 88002-5501	1
ARMY RESEARCH LABORATORY AMSRL BE ATTN MR VEAZY BATTLEFIELD ENVIR DIR WSMR NM 88002-5501	1
DTIC 8725 JOHN J KINGMAN RD SUITE 0944 FT BELVOIR VA 22060-6218	1
ARMY MISSILE CMND AMSMI REDSTONE ARSENAL AL 35898-5243	1
ARMY DUGWAY PROVING GRD STEDP 3 DUGWAY UT 84022-5000 USATRADOC ATCD FA FT MONROE VA 23651-5170	1
WSMR TECH LIBRARY BR STEWS IM IT WSMR NM 88001	1
Record Copy	2
TOTAL	81